J. Fluid Mech. (2002), *vol.* 457, *pp.* 255–283.
DOI: 10.1017/S0022112001007649 Printed in the United Kingdom

A general theory for the dynamics of thin viscous sheets

By N. M. RIBE

Institut de Physique du Globe, 4 place Jussieu, 75252 Paris cédex 05, France

(Received 20 March 2001 and in revised form 11 October 2001)

A model for the deformation of thin viscous sheets of arbitrary shape subject to arbitrary loading is presented. The starting point is a scaling analysis based on an analytical solution of the Stokes equations for the flow in a shallow (nearly planar) sheet with constant thickness T_0 and principal curvatures k_1 and k_2, loaded by an harmonic normal stress with wavenumbers q_1 and q_2 in the directions of principal curvature. Two distinct types of deformation can occur: an 'inextensional' (bending) mode when $|L^3(k_1q_2^2 + k_2q_1^2)| \ll \epsilon$, and a 'membrane' (stretching) mode when $|L^3(k_1q_2^2 + k_2q_1^2)| \gg \epsilon$, where $L \equiv (q_1^2 + q_2^2)^{-1/2}$ and $\epsilon = T_0/L \ll 1$. The scales revealed by the shallow-sheet solution together with asympotic expansions in powers of ϵ are used to reduce the three-dimensional equations for the flow in the sheet to a set of equivalent two-dimensional equations, valid in both the inextensional and membrane limits, for the velocity $\boldsymbol{U}$ of the sheet midsurface. Finally, kinematic evolution equations for the sheet shape (metric and curvature tensors) and thickness are derived. Illustrative numerical solutions of the equations are presented for a variety of buoyancy-driven deformations that exhibit buckling instabilities. A collapsing hemispherical dome with radius L deforms initially in a compressional membrane mode, except in bending boundary layers of width $\sim (\epsilon L)^{1/2}$ near a clamped equatorial edge, and is unstable to a buckling mode which propagates into the dome from that edge. Buckling instabilities are suppressed by the extensional flow in a sagging inverted dome (pendant drop), which consequently evolves entirely in the membrane mode. A two-dimensional viscous jet falling onto a rigid plate exhibits steady periodic folding, the frequency of which varies with the jet height and extrusion rate in a way similar to that observed experimentally.

1. Introduction

Thin, highly deformable viscous sheets occur frequently both in technological applications and in nature. In glass and plastics manufacture, sheets of liquid polymer are deformed by applied loads chosen such that the sheet achieves some desired shape (such as that of a bottle or an automobile windshield) before solidifying. A comprehensive survey of such processes, which include film blowing, blow moulding, and extrusion, can be found in Pearson (1985). On a different scale, the Earth's outer shell (lithosphere) can be regarded as an assemblage of thin viscous sheets with characteristic thickness $\sim$ 100 km and lateral dimension $\sim$ 1000–10 000 km. The mutual interactions of these sheets ('plates') produces collisional mountain ranges such as the Himalayas, and initiates the sinking or 'subduction' of oceanic plates into the mantle below. Images of subducted plates obtained using seismic tomography (Hilst, Widyantoro &

Engdahl 1997) suggest that they undergo complex deformations during their descent, which may in some cases extend to the core–mantle boundary (2900 km depth).

The aim of this paper is to derive a general theory that can predict how a thin viscous sheet of arbitrary shape responds to arbitrary applied loads. The primary factor that controls this response is the sheet curvature. This fact can be appreciated by recalling some well-known examples of the behaviour of thin elastic shells, which are closely analogous (*modulo* a time derivative) to viscous sheets. The enormous resistance of an eggshell to longitudinal compression, for example, was noted with wonder by several writers of classical antiquity (Benvenuto 1991, p. 312). Similarly, it was recognized very early that arches and domes could span a much wider space than a flat roof of the same thickness. In short, curvature provides strength. We now know that this is so because shells respond to loads in two fundamentally different ways: by bending, and by stretching/shortening (the 'membrane' response). High curvature favours a membrane state that is inherently less susceptible to failure than one dominated by bending, in which large tensional stresses are generated on the side of the shell away from the centre of bending. Discussions of these points can be found in most textbooks on elastic shell theory (e.g. Novozhilov 1959; Goldenveizer 1961; Calladine 1983; Niordson 1985; Libai & Simmonds 1998; Ciarlet 1999).

The theory of viscous sheets is much less developed than that of elastic shells. Beginning with the classic papers of Pearson & Petrie (1970*a*, *b*), early viscous sheet theories focused on the industrial process of film blowing, in which a viscous sheet inflated by an applied excess pressure deforms by stretching alone. Fliert, Howell & Ockendon (1995) derived general equations for unsteady blowing of films with arbitrary shape, and gave detailed references to previous work. Theories that incorporate both stretching and bending include those of Buckmaster, Nachman & Ting (1975) and Ribe (2001); but both are limited to two dimensions. Howell (1996) derived general equilibrium equations for three-dimensional membrane sheets in lines-of-curvature coordinates, and Howell (1999) extended these by using general coordinates and incorporating surface tension. However, neither study considered bending modes. A fully general theory for three-dimensional sheets that deform by both stretching and bending does not yet exist.

The focus of this study is on thin or slender sheets whose characteristic thickness is much smaller than the lateral length scale of their deformation. The goal is to reduce the full three-dimensional equations of viscous flow to equivalent two-dimensional equations for the motion of the sheet 'midsurface' that are valid asymptotically in the limit of small slenderness. The starting point is an analytical solution of a simplified set of equations for 'shallow' (nearly planar) sheets, which shows at a glance the relative roles of stretching and bending and the scalings associated with each. Next, these scalings are used as the basis for systematic asymptotic expansions from which composite thin-sheet constitutive relations are determined that are valid for arbitrary sheets deforming by either stretching or bending. The resulting thin-sheet equations, complemented by kinematic equations describing the evolution of the sheet thickness and shape, are then solved numerically for several illustrative model problems.

An essential aspect of the derivation herein is the description of the sheet midsurface using general non-orthogonal coordinates, rather than orthogonal 'lines-of-curvature' coordinates that follow the directions of principal curvature of the midsurface. Lines-of-curvature coordinates are perfectly adequate for the 'quasi-static' problem of determining the instantaneous flow in a sheet of a given shape subject to given applied loads (e.g. Howell 1996). However, because a viscous sheet can experience large deformations, material coordinate lines that are initially orthogonal will not in

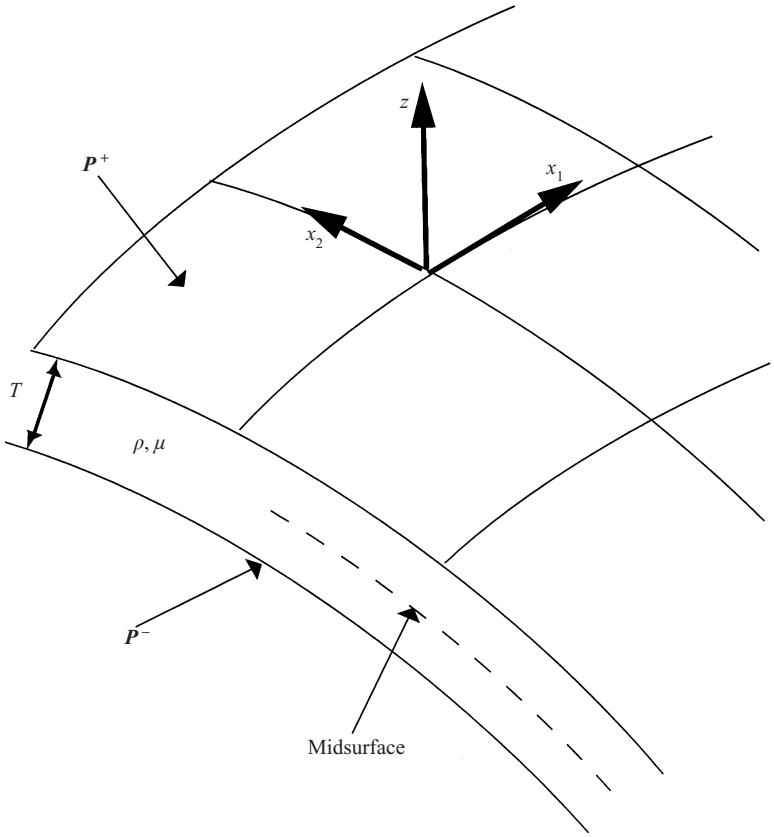

FIGURE 1. Definition sketch of the model. A viscous sheet has constant viscosity μ, constant excess density ρ, and variable thickness $T(x_1, x_2, t)$, where x_1 and x_2 are general non-orthogonal coordinates on the sheet midsurface $z = 0$ and t is time. Creeping (inertialess) flow in the sheet is driven by buoyancy, by stresses $\boldsymbol{P}^{\pm}$ applied to the outer surfaces $z = \pm T/2$, and by uniform surface tension.

general remain so. The use of lines-of-curvature coordinates in such a situation would require numerical remeshing at every time step, which is clearly impractical. General coordinates avoid this problem by allowing the use of an arbitrary coordinate grid that deforms along with the sheet.

2. Model geometry

Consider a fluid sheet with constant viscosity μ, constant excess density ρ relative to an ambient fluid, and variable thickness T (figure 1). Define the sheet 'midsurface' as the surface such that normals to it intersect the sheet outer surfaces at equal distances $T/2$. Points in the sheet will be identified by their so-called 'normal' coordinates x_i, where $x_3 \equiv z$ is the normal distance from the midsurface and x_1 and x_2 are arbitrary coordinates on the midsurface. Flow in the sheet is driven by buoyancy, by stresses $\boldsymbol{P}^{\pm}$ applied to its outer surfaces $z = \pm T/2$, and by surface tension.

Let T_0 be the characteristic thickness of the sheet, so that $T/T_0 \equiv \hat{T}(x_1, x_2, t)$ is a function of order unity. Here and henceforth, a superposed hat denotes a dimensionless variable. The sheet is 'thin' if $\epsilon \equiv T_0/L \ll 1$, where L is the smallest

lateral length scale (radius of curvature or characteristic wavelength of the applied load).

Because x_1 and x_2 are non-orthogonal coordinates, the formalism of differential geometry and general tensor calculus is required to describe the sheet shape. The following brief review uses, to the extent possible, the notation of Green & Zerna (1992, henceforth referred to as GZ), chapters 1 and 10 of which may be consulted for more detail. Throughout this paper, Latin indices range over the values 1, 2, and 3, Greek indices range over the values 1 and 2 only, and the summation convention for repeated indices (subscript/superscript pairs) is assumed.

Let $\boldsymbol{r}_0(x_1, x_2, t)$ be the position vector of a point on the midsurface relative to an arbitrary origin, and let $\boldsymbol{a_3}(x_1, x_2, t)$ be a unit vector normal to the midsurface. Then the position vector of an arbitrary point in the sheet is

$$\boldsymbol{r}(x_1, x_2, z, t) = \boldsymbol{r}_0(x_1, x_2, t) + z\boldsymbol{a}_3(x_1, x_2, t). \tag{2.1}$$

Because the coordinates x_1 and x_2 may be non-orthogonal, one must distinguish between covariant and contravariant components of vectors and tensors defined on the midsurface. The covariant midsurface basis vectors are

$$\boldsymbol{a}_\alpha = \boldsymbol{r}_{0,\alpha}, \tag{2.2}$$

where a comma denotes partial differentiation with respect to x_α. The contravariant basis vectors $\boldsymbol{a}^\alpha$ are just the reciprocals of the covariant ones, and satisfy

$$\boldsymbol{a}^\alpha \cdot \boldsymbol{a}_\beta = \delta^\alpha_\beta, \tag{2.3}$$

where δ^α_β is the Kronecker delta. The quantities

$$a_{\alpha\beta} = \boldsymbol{a}_\alpha \cdot \boldsymbol{a}_\beta, \quad a^{\alpha\beta} = \boldsymbol{a}^\alpha \cdot \boldsymbol{a}^\beta, \tag{2.4}$$

are respectively the covariant and contravariant components of the (symmetric) metric tensor of the midsurface.

The second fundamental tensor of the midsurface is its curvature tensor, with covariant components

$$b_{\alpha\beta} = -\boldsymbol{a}_\alpha \cdot \boldsymbol{a}_{3,\beta} = -\boldsymbol{a}_\beta \cdot \boldsymbol{a}_{3,\alpha}. \tag{2.5}$$

These are related to the mixed components b^α_β and contravariant components $b^{\alpha\beta}$ by the formulae

$$b^\alpha_\beta = a^{\alpha\lambda}b_{\beta\lambda} = a_{\beta\lambda}b^{\alpha\lambda}, \quad b^{\alpha\beta} = a^{\alpha\lambda}b^\beta_\lambda, \quad b_{\alpha\beta} = a_{\alpha\lambda}b^\lambda_\beta, \tag{2.6}$$

illustrating the general rule that inner multiplication of a surface vector or tensor by $a^{\alpha\beta}$ (or $a_{\alpha\beta}$) is equivalent to raising (or lowering) the appropriate index. The invariant quantities

$$H = \tfrac{1}{2}b^\alpha_\alpha, \quad G = b^1_1 b^2_2 - b^1_2 b^2_1, \tag{2.7}$$

are respectively the mean curvature and the Gaussian curvature of the midsurface. A third invariant quantity that will prove useful is the 'curvature modulus'

$$K \equiv (4H^2 - 2G)^{1/2} = (b^\alpha_\beta b^\beta_\alpha)^{1/2}. \tag{2.8}$$

The mutually perpendicular principal directions of the curvature tensor are those with respect to which the midsurface is not twisted, i.e. along which adjacent normals to the midsurface are coplanar. The principal values k_1 and k_2 of b^α_β are the 'principal curvatures' of the midsurface. In terms of these, the three invariant quantities defined

above are

$$H = \frac{k_1 + k_2}{2}, \quad G = k_1 k_2, \quad K = (k_1^2 + k_2^2)^{1/2}. \tag{2.9}$$

Because the sheet is curved, the base vectors $\boldsymbol{r}_{,\alpha}$ at points off the midsurface are not identical to the midsurface base vectors $\boldsymbol{r}_{0,\alpha}$ (see (2.1)). The covariant base vectors $\boldsymbol{g}_i$ and the contravariant base vectors $\boldsymbol{g}^i$ at an arbitrary point in the sheet are

$$\boldsymbol{g}_\alpha \equiv \boldsymbol{r}_{,\alpha} = \mu_\alpha^\lambda \boldsymbol{a}_\lambda, \quad \boldsymbol{g}^\alpha = h^{-1}(\mu_\rho^\rho \delta_\lambda^\alpha - \mu_\lambda^\alpha)\boldsymbol{a}^\lambda, \quad \boldsymbol{g}_3 = \boldsymbol{g}^3 = \boldsymbol{a}_3, \tag{2.10}$$

where

$$\mu_\alpha^\beta = \delta_\alpha^\beta - z b_\alpha^\beta \tag{2.11}$$

and

$$h = 1 - 2Hz + Gz^2 \tag{2.12}$$

is the ratio of an element of surface area at a distance z from the midsurface to the corresponding area on the midsurface itself. The covariant and contravariant components of the metric tensor at an arbitrary point in the sheet are

$$g_{ij} = \boldsymbol{g}_i \cdot \boldsymbol{g}_j, \quad g^{ij} = \boldsymbol{g}^i \cdot \boldsymbol{g}^j. \tag{2.13}$$

To apply boundary conditions, we shall require a final set of basis vectors that are respectively tangential and normal to the sheet outer surfaces

$$\boldsymbol{r}^\pm = \boldsymbol{r}_0 \pm \tfrac{1}{2} T \boldsymbol{a}_3. \tag{2.14}$$

Here and henceforth, $\pm$ (placed as a subscript or superscript as convenient) indicates that the variable in question is evaluated at $z = \pm T/2$. The covariant and contravariant tangent vectors to the outer surfaces are

$$\boldsymbol{c}_\alpha^\pm \equiv \pm \boldsymbol{r}_{,\alpha}^\pm = \pm \boldsymbol{g}_\alpha^\pm + \tfrac{1}{2} T_{,\alpha} \boldsymbol{g}_3, \quad \boldsymbol{c}_\pm^\alpha = \pm \boldsymbol{g}_\pm^\alpha + \frac{g^{\alpha\lambda} T_{,\lambda}}{2\Lambda_\pm^2}(\boldsymbol{g}^3 \mp \tfrac{1}{2} T_{,\beta} \boldsymbol{g}_\pm^\beta), \tag{2.15}$$

where

$$\Lambda_\pm = \left(1 + \tfrac{1}{4} g_\pm^{\alpha\beta} T_{,\alpha} T_{,\beta}\right)^{1/2}. \tag{2.16}$$

The (outward) unit normal vectors $\boldsymbol{c}_3^\pm = \boldsymbol{c}_\pm^3 \equiv \boldsymbol{n}^\pm$ are then

$$\boldsymbol{n}^\pm = \frac{\boldsymbol{c}_1^\pm \times \boldsymbol{c}_2^\pm}{|\boldsymbol{c}_1^\pm \times \boldsymbol{c}_2^\pm|} = n_i^\pm \boldsymbol{g}_\pm^i, \quad (n_\alpha^\pm, n_3^\pm) = \Lambda_\pm^{-1}(-\tfrac{1}{2} T_{,\alpha}, \pm 1). \tag{2.17}$$

Note that if T is constant, $\boldsymbol{c}_i^\pm = \pm \boldsymbol{g}_i^\pm$ and $\boldsymbol{c}_\pm^i = \pm \boldsymbol{g}_\pm^i$. The mean curvatures of the outer surfaces are

$$H_\pm = H \pm \tfrac{1}{4}(K^2 T + a^{\alpha\beta} T|_{\alpha\beta}) + O(\epsilon^2 L^{-1}). \tag{2.18}$$

A final important notion from differential geometry is that of covariant differentiation with respect to the midsurface coordinates x_α. The covariant derivative of a vector (or tensor) component is just the corresponding component of the partial derivative of the vector (or tensor) itself, taking into account the variation of the basis vectors from point to point. Because the covariant derivatives of all components of the metric tensor are zero, the covariant derivative may be thought of as a derivative that follows the changing metric of a surface. Expressions for the covariant derivatives of surface vectors and tensors are given in chapter 1 of GZ. In what follows, these derivatives will be denoted by a vertical line; thus $u_\alpha|_\beta$ is the covariant derivative of u_α with respect to x_β.

3. Governing equations and boundary conditions

In the theory of thin sheets, the fundamental dynamic quantities are the stress resultants and bending moments, defined as (weighted) integrals of the stresses across the sheet. For these integrals to be meaningful, the stresses must be expressed both per unit area of a single reference surface and relative to base vectors that do not vary across the sheet. The natural choice for this purpose is the midsurface and its intrinsic base vectors $\boldsymbol{a}_i$. The stress tensor referred to the midsurface in this way is (GZ, p. 375)

$$\sigma^{i\lambda} = h\mu^{\lambda}_{\alpha}\tau^{i\alpha}, \quad \sigma^{i3} = h\tau^{i3}, \tag{3.1}$$

where τ^{ij} is the stress tensor per unit *local* area and relative to the *local* basis $\boldsymbol{g}_i$. The tensor σ^{ij} is not symmetric.

The equations of equilibrium in terms of σ^{ij} are (GZ, p. 379)

$$\sigma^{\alpha\beta}|_{\alpha} - b^{\beta}_{\alpha}\sigma^{\alpha 3} + \sigma^{3\beta}_{,3} = -h\rho f^{\beta}, \tag{3.2a}$$

$$\sigma^{\alpha 3}|_{\alpha} + b_{\alpha\beta}\sigma^{\alpha\beta} + \sigma^{33}_{,3} = -h\rho f^{3}, \tag{3.2b}$$

where $f^i\boldsymbol{a}_i$ is the gravitational acceleration. The constitutive relations for a Newtonian fluid are

$$\tau^{ij} = -pg^{ij} + 2\mu g^{ik}g^{jl}e_{kl}, \tag{3.3}$$

where p is the pressure and e_{ij} is the strain rate tensor given by (GZ, p. 381)

$$2e_{\alpha\beta} = \mu^{\lambda}_{\beta}(u_{\lambda}|_{\alpha} - b_{\lambda\alpha}u_3) + \mu^{\lambda}_{\alpha}(u_{\lambda}|_{\beta} - b_{\lambda\beta}u_3) \tag{3.4a}$$

$$2e_{\alpha 3} = u_{3,\alpha} + u_{\alpha,3} + b^{\lambda}_{\alpha}(u_{\lambda} - zu_{\lambda,3}), \tag{3.4b}$$

$$e_{33} = u_{3,3}. \tag{3.4c}$$

Finally, incompressibility of the fluid requires $g^{ij}e_{ij} = 0$, or equivalently

$$(hu_3)_{,3} + [a^{\alpha\beta} + z(b^{\alpha\beta} - 2Ha^{\alpha\beta})]u_{\alpha}|_{\beta} = 0. \tag{3.5}$$

3.1. *Global force and torque balance*

Equations for global force balance are obtained by integrating (3.2*a*) and (3.2*b*) across the sheet, yielding

$$n^{\alpha\beta}|_{\alpha} - b^{\beta}_{\alpha}q^{\alpha} + \mathscr{P}^{\beta} = 0, \tag{3.6a}$$

$$q^{\alpha}|_{\alpha} + b_{\alpha\beta}n^{\alpha\beta} + \mathscr{P}^{3} = 0, \tag{3.6b}$$

where

$$n^{\alpha\beta} = \int_{-T/2}^{T/2} \sigma^{\alpha\beta}\,\mathrm{d}z, \quad q^{\alpha} = \int_{-T/2}^{T/2} \sigma^{\alpha 3}\,\mathrm{d}z \tag{3.7}$$

are 'stress resultant' tensors,

$$\mathscr{P}^{j} = f^{j}\int_{-T/2}^{T/2} \rho h\,\mathrm{d}z + \mathscr{F}^{j}_{+} + \mathscr{F}^{j}_{-}, \tag{3.8}$$

and

$$\mathscr{F}^{j}_{\pm} = \Lambda_{\pm}\sigma^{ij}_{\pm}n^{\pm}_{i} \tag{3.9}$$

are the components of stress applied in the directions $\boldsymbol{a}_j$ to the sheet outer surface, but measured per unit area of the midsurface. The normal vector $n^{\pm}_i$ (1 Latin subscript) should not be confused with the stress resultant tensor $n^{\alpha\beta}$ (two Greek superscripts).

The equation for global torque balance is obtained by multiplying (3.2*a*) by z and then integrating, yielding

$$m^{\alpha\beta}|_\alpha - q^\beta + \mathscr{M}^\beta = 0, \tag{3.10}$$

where

$$m^{\alpha\beta} = \int_{-T/2}^{T/2} \sigma^{\alpha\beta} z \, \mathrm{d}z, \tag{3.11}$$

is the 'bending moment' tensor and

$$\mathscr{M}^\beta = f^\beta \int_{-T/2}^{T/2} \rho h z \, \mathrm{d}z + \frac{T}{2}(\mathscr{F}_+^\beta - \mathscr{F}_-^\beta) \tag{3.12}$$

is the applied moment vector.

The global force balance equations (3.6) can now be simplified by using (3.10) to eliminate q^β and by introducing (symmetric) 'effective' stress resultant and bending moment tensors (Budiansky & Sanders 1967; Niordson 1985)

$$N^{\alpha\beta} = n^{\alpha\beta} + b_\lambda^\beta m^{\lambda\alpha}, \quad M^{\alpha\beta} = \tfrac{1}{2}(m^{\alpha\beta} + m^{\beta\alpha}). \tag{3.13}$$

The resulting equations are

$$N^{\alpha\beta}|_\alpha - 2b_\lambda^\beta M^{\lambda\alpha}|_\alpha - b_\lambda^\beta|_\alpha M^{\lambda\alpha} + \mathscr{P}^\beta - b_\alpha^\beta \mathscr{M}^\alpha = 0, \tag{3.14a}$$

$$M^{\alpha\beta}|_{\alpha\beta} - b_{\alpha\lambda} b_\beta^\lambda M^{\alpha\beta} + b_{\alpha\beta} N^{\alpha\beta} + \mathscr{P}^3 + \mathscr{M}^\alpha|_\alpha = 0. \tag{3.14b}$$

3.2. *Boundary conditions*

Let

$$\boldsymbol{P}^\pm = P_i^\pm \boldsymbol{c}_\pm^i = P_\pm^i \boldsymbol{c}_i^\pm \tag{3.15}$$

be the vector stress applied to the outer surfaces of the sheet, per unit areas of those surfaces (*not* of the midsurface). Thus $P_\alpha^\pm$ or $P_\pm^\alpha$ are the tangential components of the applied stress, and $P_3^\pm = P_\pm^3$ are the normal components. Continuity of stress at the outer surfaces then requires

$$\tau_\pm^{ij} n_i^\pm \boldsymbol{g}_j^\pm = \boldsymbol{P}^\pm \pm 2\gamma H_\pm \boldsymbol{n}^\pm, \tag{3.16}$$

where γ is the coefficient of surface tension (assumed constant). Recall that the boundary stresses appear in the global force balance equations only in the combinations $\mathscr{F}_\pm^j$ defined by (3.9). Expressions for these quantities in terms of the components of $\boldsymbol{P}^\pm$ are obtained by projecting (3.16) onto the base vectors $\boldsymbol{a}^3$ and $\boldsymbol{a}^\alpha$, yielding

$$\mathscr{F}_\pm^3 = h_\pm(\pm P_\pm^3 + 2\gamma H_\pm) + \tfrac{1}{2} T_{,\alpha} P_\pm^\alpha + O(\epsilon^2 |\boldsymbol{P}|), \tag{3.17a}$$

$$\mathscr{F}_\pm^\alpha = \pm h_\pm P_\pm^\alpha - \tfrac{1}{2} T b_\beta^\alpha P_\pm^\beta - \tfrac{1}{2} a^{\alpha\beta} T_{,\beta}(P_\pm^3 \pm 2\gamma H_\pm) + O(\epsilon^2 |\boldsymbol{P}|). \tag{3.17b}$$

4. 'Shallow-sheet' scaling analysis

Let us first develop an intuitive understanding of how viscous sheets respond to applied loads. Consider a 'shallow' sheet of constant thickness T_0 whose midsurface departs from a reference plane by an amount much smaller than its principal radii of curvature. The metric tensor for such a sheet is nearly equal to that of a plane. Accordingly, the equations governing the flow in a shallow sheet can be simplified by neglecting the effects of curvature on the metric tensor while retaining them elsewhere in the equilibrium equations. Such an approximation is consistent because the former

effects are proportional to the square of the curvature, whereas the latter are linear in the curvature. The solution presented below corresponds to a more accurate version of the Donnell–Mushtari–Vlasov theory of shallow elastic shells (Niordson 1985, chap. 15).

Let x_α be orthogonal 'lines-of-curvature' coordinates parallel to the directions of the principal curvatures $b^1_1 \equiv k_1$ and $b^2_2 \equiv k_2$ of the midsurface. The components of the metric tensor of the sheet are approximately $a_{11} = a_{22} = 1$, $a_{12} = a_{21} = 0$. If we suppose further that k_1 and k_2 are constant, then the coefficients of the continuity and momentum equations become independent of x_1 and x_2. Consider the flow driven by a normal stress $P \cos q_1 x_1 \cos q_2 x_2$ applied to the upper surface $z = T_0/2$, and suppose for simplicity that the lower surface $z = -T_0/2$ is stress-free. Then the velocity components $(u_1, u_2, u_3) \equiv (u, v, w)$ and the pressure p within the sheet have the forms

$$u = \frac{PL}{\mu} \sin q_1 x_1 \cos q_2 x_2 \sum_{j=0}^{J} u_j \hat{z}^j, \quad v = \frac{PL}{\mu} \cos q_1 x_1 \sin q_2 x_2 \sum_{j=0}^{J} v_j \hat{z}^j, \tag{4.1a}$$

$$w = \frac{PL}{\mu} \cos q_1 x_1 \cos q_2 x_2 \sum_{j=0}^{J} w_j \hat{z}^j, \quad p = P \cos q_1 x_1 \cos q_2 x_2 \sum_{j=0}^{J-1} p_j \hat{z}^j, \tag{4.1b}$$

where $L \equiv (q_1^2 + q_2^2)^{-1/2}$ is the wavelength of the applied load, $\hat{z} = z/T_0$, and u_j, v_j, w_j and p_j are dimensionless coefficients. A value $J = 4$ is sufficient to predict correctly all quantities of interest in the thin-sheet limit $\epsilon \to 0$.

Substitution of (4.1) into the governing equations (3.2)–(3.5) and the boundary conditions (3.16) with $P^j_- = \gamma = 0$ and $P^j_+ = P\delta^j_3$ yields a set of nineteen linear algebraic equations for the coefficients u_j, v_j, w_j and p_j. In writing the solutions, it is convenient to define dimensionless curvatures $(\mathscr{K}_1, \mathscr{K}_2) = L(k_1, k_2)$ and dimensionless wavenumbers $(\mathscr{Q}_1, \mathscr{Q}_2) = L(q_1, q_2)$, where $\mathscr{Q}_1^2 + \mathscr{Q}_2^2 = 1$ by virtue of the definition of L. Also, let $\mathscr{G} \equiv \mathscr{K}_1\mathscr{K}_2$, $\mathscr{H} \equiv (\mathscr{K}_1 + \mathscr{K}_2)/2$, and $\mathscr{K} \equiv (\mathscr{K}_1^2 + \mathscr{K}_2^2)^{1/2}$ be the dimensionless Gaussian curvature, mean curvature, and curvature modulus, respectively, of the midsurface.

The solutions required for our purposes are

$$w_0 = \frac{3}{\epsilon \Delta}, \tag{4.2a}$$

$$u_0 = \frac{3\mathscr{Q}_1[2(\mathscr{K}_1 - \mathscr{K}_2) + 3\mathscr{I}]}{2\epsilon\Delta}, \tag{4.2b}$$

$$u_1 = -\frac{3\mathscr{Q}_1[2(\mathscr{K}_1^2 - \mathscr{G} - 1) + 3(\mathscr{K}_1^2\mathscr{Q}_2^2 + \mathscr{G}\mathscr{Q}_1^2)]}{2\Delta}, \tag{4.2c}$$

$$p_0 = \frac{6\mathscr{I} + \epsilon^2\mathscr{H}(3\mathscr{K}^2 - \mathscr{G} - 3)}{2\epsilon\Delta}, \tag{4.2d}$$

$$p_1 = -\frac{3[2 - 2\mathscr{I}\mathscr{H} + 3\mathscr{I}^2 - 2\mathscr{K}^2]}{\Delta}, \tag{4.2e}$$

where

$$\mathscr{I} = \mathscr{K}_1\mathscr{Q}_2^2 + \mathscr{K}_2\mathscr{Q}_1^2, \tag{4.2f}$$

$$\Delta = 9\mathscr{I}^2 + \epsilon^2[(1 - \mathscr{K}^2)^2 + \mathscr{G}(1 - \mathscr{K}^2 + \mathscr{G})] \tag{4.2g}$$

The solutions for v_0 and v_1 are obtained from those for u_0 and u_1 by interchanging the subscripts 1 and 2. In reality, each of the numerators and denominators of (4.2*a–g*) is an infinite power series in ϵ, of which only the leading terms are shown.

The two terms in the denominator Δ correspond to the membrane and inextensional modes of deformation. In the membrane limit, the first term is dominant, and the sheet responds to a load by stretching ($w_0 \sim \epsilon^{-1}$). The second term is dominant in the inextensional limit, where the sheet responds by bending ($w_0 \sim \epsilon^{-3}$). In general, a sheet responds to a load by both mechanisms. The relative importance of the bending response can be measured by a 'dissipation number' D ($0 \leqslant D \leqslant 1$), defined as the ratio of the rate of energy dissipation due to bending to the total (bending plus stretching) dissipation rate. Direct calculation using the shallow-sheet solution yields

$$D = \frac{\epsilon^2 f(\mathscr{K}, \mathscr{G}, \phi)}{\mathscr{I}^2 + \epsilon^2 f(\mathscr{K}, \mathscr{G}, \phi)}, \tag{4.3}$$

where f is a function of $\mathscr{K}$, $\mathscr{G}$, and $\phi \equiv \tan^{-1}(\mathscr{Q}_2/\mathscr{Q}_1)$ that is of order unity in the limit $\mathscr{K} \to 0$. The angle ϕ ranges from 0 when the load varies only in the x_1-direction to $\pi/2$ when it varies only in the x_2-direction. Equation (4.3) shows that loaded viscous sheets deform primarily by stretching when $|\mathscr{I}| > \epsilon$, and primarily by bending when $|\mathscr{I}| < \epsilon$.

Figure 2 shows D as a function of ϕ and the 'reduced Gaussian curvature' $r = \mathscr{G}/\mathscr{K}^2 = G/K^2$, for three values of $\mathscr{K}$ and $\epsilon = 0.01$. The parameter r spans the entire range of Gaussian curvature, from $r = -1/2$ for a catenoidal sheet to $r = 0$ for a flat or cylindrical sheet to $r = 1/2$ for a spherical sheet. Figure 2 shows that $\mathscr{K} = \epsilon$ is the 'critical' curvature modulus for which stretching and bending are of roughly equal importance. In general, $\mathscr{K} > \epsilon$ favours stretching and $\mathscr{K} < \epsilon$ favours bending, except in the neighbourhood of an 'inextensional' line $\sin^2\phi = k_2/(k_2 - k_1)$ (black lines in figure 2), where $\mathscr{I}$ vanishes. Along this line, the sheet responds to the applied load by bending no matter how large $\mathscr{K}$ may be. The existence of the inextensional line explains the fact, well known to structural engineers, that the behaviour of elastic shells with negative Gaussian curvature often cannot be adequately modelled using membrane theory alone. It is important to note that inextensionality depends both on the sheet geometry and on the loading distribution. For example, a cylindrical sheet ($r = 0$) is inextensional if the loading varies only in the azimuthal direction ($\phi = 0$), but not if it varies also in the axial direction.

The shallow-sheet solution obtained above reveals how the variables u, v, w and p scale as functions of ϵ. The solutions show, first, that the quadratic terms u_2, v_2 and p_2 are always small relative to the corresponding constant terms (u_0, v_0, p_0) and linear terms (u_1, v_1, p_1). Accordingly, the scales for u, v and p are $\max(u_0, u_1)$, $\max(v_0, v_1)$, and $\max(p_0, p_1)$, respectively. Second, because $w_0 \gg w_1, w_2$, the scale for w is simply that for w_0. There are two distinct scaling regimes, according to whether the first or the second term in (4.2*g*) is dominant. Suppose first that $\mathscr{I} = O(1)$, so that the second (bending) term in (4.2*g*) is negligible. Assuming $\mathscr{K} = O(1)$, we obtain the 'membrane' scaling

$$u, v, w \sim \frac{PL}{\mu}\epsilon^{-1}, \quad p \sim P\epsilon^{-1}. \tag{4.4}$$

If on the other hand $|\mathscr{I}| \ll \epsilon$, we find the 'inextensional' scaling

$$u, v, w \sim \frac{PL}{\mu}\epsilon^{-3}, \quad p \sim P\epsilon^{-2}. \tag{4.5}$$

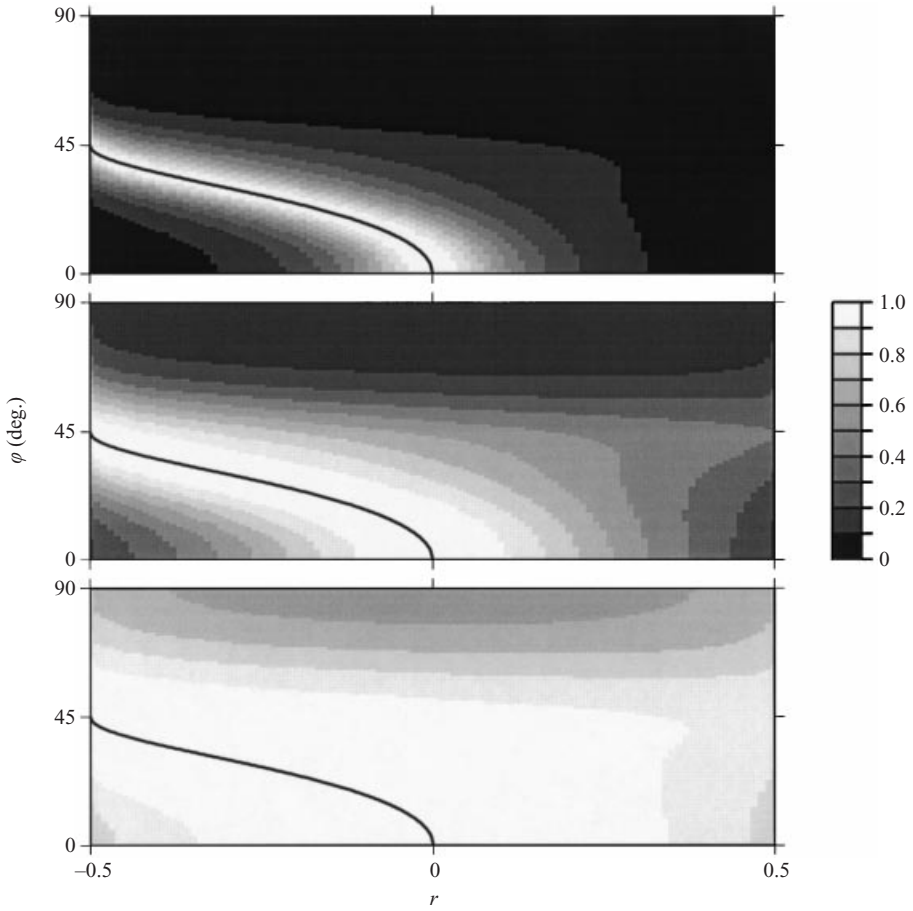

FIGURE 2. Dissipation number (4.3) for an harmonically loaded shallow sheet as a function of reduced Gaussian curvature $r = G/K^2$ and $\phi = \tan^{-1}(Q_2/Q_1)$, for $\epsilon = 0.01$ and $\mathscr{K}/\epsilon = 0.3$ (bottom), $\mathscr{K}/\epsilon = 1.0$ (middle), and $\mathscr{K}/\epsilon = 3.0$ (top). Black line is the inextensional line $\mathscr{I} = 0$.

The assumption $\mathscr{K} = O(1)$ used to obtain the scales (4.4) and (4.5) is not strictly speaking consistent with the shallow-sheet approximation, which requires the dimensionless curvatures to be small. To test the validity of (4.4) and (4.5), I determined exact analytical solutions for the flow in harmonically loaded cylindrical and spherical sheets of constant thickness. These solutions show directly that the scales (4.4) and (4.5) are correct for sheets with arbitrary curvature up to $\mathscr{K} = O(1)$.

5. Thin-sheet constitutive relations

The next step is to determine the appropriate constitutive relations for thin viscous sheets. In the limit $\epsilon \to 0$, a viscous sheet behaves as a surface of effectively zero thickness with finite resistances to stretching and bending, measured respectively by the stress resultant and bending moment tensors $N^{\alpha\beta}$ and $M^{\alpha\beta}$. The thin-sheet constitutive relations specify how $N^{\alpha\beta}$ and $M^{\alpha\beta}$ depend on the two tensors that describe the rate of deformation of the midsurface: the strain rate tensor

$$\Delta_{\alpha\beta} = \tfrac{1}{2}(U_\alpha|_\beta + U_\beta|_\alpha) - b_{\alpha\beta}U_3 \tag{5.1}$$

and the rate of change of curvature tensor

$$\Omega_{\alpha\beta} = U_3|_{\alpha\beta} - b^{\lambda}_{\alpha} b_{\lambda\beta} U_3 + b^{\lambda}_{\alpha} U_{\lambda}|_{\beta} + b^{\lambda}_{\beta} U_{\lambda}|_{\alpha} + b^{\lambda}_{\beta}|_{\alpha} U_{\lambda}, \tag{5.2}$$

where $U_i \equiv u_i(z=0)$ is the fluid velocity at the midsurface. In fact, the tensors $\Delta_{\alpha\beta}$ and $\Omega_{\alpha\beta}$ need not be known in advance; they will appear naturally in the course of the asymptotic expansions below.

5.1. *Asymptotic expansion: membrane limit*

The thin-sheet constitutive relations can be determined by expanding the primitive variables u_i and p in powers of the small parameter ϵ. Related expansion techniques have long been used in elastic shell theory (e.g. Goldenveizer 1963; Sanchez-Palencia 1990). The powers of ϵ in the leading terms of these expansions are those revealed by the shallow-sheet scaling analysis of the previous section, where we saw that distinct scalings exist for membrane (stretching) and inextensional (bending) deformations. We therefore require separate asymptotic expansions for these two limits. Much unnecessary labour can be avoided by expanding u_i and p directly in double power series in ϵ and the dimensionless normal coordinate $\hat{z}$.

In view of the scalings (4.4), the appropriate expansions in the membrane limit are

$$u_i = \frac{PL}{\mu\epsilon} \sum_{m=0} \sum_{n=0} \epsilon^m \hat{z}^n u_i^{(mn)}, \quad p = \frac{P}{\epsilon} \sum_{m=0} \sum_{n=0} \epsilon^m \hat{z}^n p^{(mn)}, \tag{5.3}$$

where the coefficients $u_i^{(mn)}$ and $p^{(mn)}$ are dimensionless functions of the lateral coordinates x_α. To simplify the notation, define dimensionless curvatures $(\hat{b}_{\alpha\beta}, \hat{b}^{\beta}_{\alpha}, \hat{H}) = L(b_{\alpha\beta}, b^{\beta}_{\alpha}, H)$ and dimensionless strain rate and rate of change of curvature tensors

$$\Delta^{(n0)}_{\alpha\beta} = \tfrac{1}{2}(u^{(n0)}_{\alpha}|_{\beta} + u^{(n0)}_{\beta}|_{\alpha}) - \hat{b}_{\alpha\beta} u^{(n0)}_3, \tag{5.4a}$$

$$\Omega^{(n0)}_{\alpha\beta} = u^{(n0)}_3|_{\alpha\beta} - \hat{b}^{\lambda}_{\alpha}\hat{b}_{\lambda\beta} u^{(n0)}_3 + \hat{b}^{\lambda}_{\alpha} u^{(n0)}_{\lambda}|_{\beta} + \hat{b}^{\lambda}_{\beta} u^{(n0)}_{\lambda}|_{\alpha} + \hat{b}^{\lambda}_{\beta}|_{\alpha} u^{(n0)}_{\lambda}, \tag{5.4b}$$

which are related to the dimensional tensors $\Delta_{\alpha\beta}$ and $\Omega_{\alpha\beta}$ by

$$\Delta_{\alpha\beta} = \frac{P}{\epsilon\mu}[\Delta^{(00)}_{\alpha\beta} + \epsilon\Delta^{(10)}_{\alpha\beta} + O(\epsilon^2)], \quad \Omega_{\alpha\beta} = \frac{P}{\epsilon\mu L}[\Omega^{(00)}_{\alpha\beta} + \epsilon\Omega^{(10)}_{\alpha\beta} + O(\epsilon^2)]. \tag{5.5}$$

Flow in the sheet can be driven by buoyancy and surface tension in addition to applied surface forces. For the purposes of asymptotic expansion, I shall assume that the effective loads due to buoyancy and surface tension are of the same order as those due to surface forces. By (3.8) and (3.16), this requires

$$\rho g L \sim \epsilon^{-1} P, \quad \gamma \sim LP. \tag{5.6}$$

Now substitute the expansions (5.3) into the governing equations (3.2)–(3.5) and the boundary conditions (3.16), and require terms proportional to the same powers of ϵ and $\hat{z}$ in each equation to vanish separately. We thereby obtain a set of coupled linear algebraic equations for the coefficients $u_i^{(mn)}$ and $p^{(mn)}$ that can be solved sequentially. The leading-order expressions for the (dimensional) tensors $N^{\alpha\beta}$ and $M^{\alpha\beta}$ in terms of these coefficients are

$$\frac{N^{\alpha\beta}}{LP} = \hat{T}[2a^{\alpha\rho}a^{\beta\lambda}\Delta^{(00)}_{\rho\lambda} - a^{\alpha\beta}p^{(00)}], \tag{5.7a}$$

$$\frac{M^{\alpha\beta}}{L^2P} = -\tfrac{1}{12}\epsilon^2\hat{T}^3[a^{\alpha\beta}p^{(11)} + (\hat{b}^{\alpha\beta} - 2\hat{H}a^{\alpha\beta})p^{(00)} + 2\hat{b}^{\alpha}_{\lambda}\hat{b}^{\lambda\beta}u_3^{(00)} + 2\hat{b}^{\alpha\beta}u_3^{(11)}$$
$$-(a^{\alpha\rho}\hat{b}^{\beta\lambda} + a^{\beta\rho}\hat{b}^{\alpha\lambda})u_{\rho}^{(00)}|_{\lambda} - (a^{\alpha\rho}a^{\beta\lambda} + a^{\beta\rho}a^{\alpha\lambda})u_{\rho}^{(11)}|_{\lambda}$$
$$-(a^{\alpha\rho}\hat{b}^{\beta\lambda} + a^{\beta\rho}\hat{b}^{\alpha\lambda} - 4\hat{H}a^{\alpha\rho}a^{\beta\lambda})\Delta_{\rho\lambda}^{(00)}]. \tag{5.7b}$$

For clarity, coefficients $u_i^{(mn)}$ and $p^{(mn)}$ that will later prove to be identically zero have been omitted from the above expansions. The remaining non-zero coefficients are

$$u_{\alpha}^{(11)} = -u_{3,\alpha}^{(00)} - \hat{b}_{\alpha}^{\beta}u_{\beta}^{(00)}, \quad u_3^{(11)} = -a^{\alpha\beta}\Delta_{\alpha\beta}^{(00)}, \tag{5.8a}$$

$$p^{(00)} = -2a^{\alpha\beta}\Delta_{\alpha\beta}^{(00)}, \quad p^{(11)} = 2[a^{\alpha\beta}\Omega_{\alpha\beta}^{(00)} - \hat{b}^{\alpha\beta}\Delta_{\alpha\beta}^{(00)}]. \tag{5.8b}$$

By substituting (5.8) into (5.7) and rewriting the results in terms of dimensional variables using (5.5), we obtain

$$N^{\alpha\beta} = 4\mu T\mathscr{A}^{\alpha\beta\lambda\rho}\Delta_{\lambda\rho}, \tag{5.9a}$$

$$M^{\alpha\beta} = -\tfrac{1}{3}\mu T^3(\mathscr{A}^{\alpha\beta\lambda\rho}\Omega_{\lambda\rho} + \mathscr{B}^{\alpha\beta\lambda\rho}\Delta_{\lambda\rho}), \tag{5.9b}$$

where

$$\mathscr{A}^{\alpha\beta\lambda\rho} = \tfrac{1}{4}(a^{\alpha\lambda}a^{\beta\rho} + a^{\alpha\rho}a^{\beta\lambda}) + \tfrac{1}{2}a^{\alpha\beta}a^{\lambda\rho}, \tag{5.10a}$$

$$\mathscr{B}^{\alpha\beta\lambda\rho} = \tfrac{1}{4}[8H\mathscr{A}^{\alpha\beta\lambda\rho} - 2a^{\alpha\beta}b^{\lambda\rho} - 4a^{\lambda\rho}b^{\alpha\beta} - 3(a^{\alpha\rho}b^{\beta\lambda} + a^{\beta\rho}b^{\alpha\lambda})]. \tag{5.10b}$$

5.2. *Asymptotic expansion: inextensional limit*

The appropriate expansions for this case are

$$u_i = \frac{PL}{\mu\epsilon^3}\sum_{m=0}\sum_{n=0}\epsilon^m\hat{z}^n u_i^{(mn)}, \quad p = \frac{P}{\epsilon^2}\sum_{m=0}\sum_{n=0}\epsilon^m\hat{z}^n p^{(mn)}. \tag{5.11}$$

The dimensional strain rate and rate of change of curvature tensors have the expansions

$$\Delta_{\alpha\beta} = \frac{P}{\epsilon\mu}[\Delta_{\alpha\beta}^{(20)} + \epsilon\Delta_{\alpha\beta}^{(30)} + O(\epsilon^2)], \quad \Omega_{\alpha\beta} = \frac{P}{\epsilon^3\mu L}[\Omega_{\alpha\beta}^{(00)} + \epsilon\Omega_{\alpha\beta}^{(10)} + O(\epsilon^2)], \tag{5.12}$$

where the results

$$\Delta_{\alpha\beta}^{(00)} = \Delta_{\alpha\beta}^{(10)} = 0, \tag{5.13}$$

implying that the sheet is inextensional to order ϵ^2, have been anticipated. The leading-order expressions for the moments are

$$\frac{N^{\alpha\beta}}{LP} = \hat{T}[2a^{\alpha\rho}a^{\beta\lambda}\Delta_{\rho\lambda}^{(20)} - a^{\alpha\beta}p^{(10)}]$$
$$+\frac{\hat{T}^3}{12}\{2(\hat{H}a^{\alpha\beta} - \hat{b}^{\alpha\beta})p^{(01)} - a^{\alpha\beta}p^{(12)} - 4\hat{H}\hat{b}^{\alpha}_{\lambda}\hat{b}^{\lambda\beta}u_3^{(00)} - 2\hat{b}^{\alpha\beta}u_3^{(22)}$$
$$+[a^{\alpha\lambda}\hat{b}^{\beta\rho} + a^{\beta\lambda}\hat{b}^{\alpha\rho} - 2a^{\alpha\rho}(\hat{H}a^{\beta\lambda} - \hat{b}^{\beta\lambda}) - 2a^{\alpha\lambda}(\hat{H}a^{\beta\rho} - \hat{b}^{\beta\rho})]u_{\rho}^{(11)}|_{\lambda}$$
$$+2\hat{H}(a^{\alpha\rho}\hat{b}^{\beta\lambda} + a^{\beta\rho}\hat{b}^{\alpha\lambda})u_{\rho}^{(00)}|_{\lambda}\}, \tag{5.14a}$$

$$\frac{M^{\alpha\beta}}{L^2P} = -\frac{\hat{T}^3}{12}[a^{\alpha\beta}p^{(01)} - (a^{\alpha\rho}\hat{b}^{\beta\lambda} + a^{\beta\rho}\hat{b}^{\alpha\lambda})u_{\rho}^{(00)}|_{\lambda}$$
$$+2\hat{b}^{\alpha}_{\lambda}\hat{b}^{\lambda\beta}u_3^{(00)} - (a^{\alpha\rho}a^{\beta\lambda} + a^{\beta\rho}a^{\alpha\lambda})u_{\rho}^{(11)}|_{\lambda}]. \tag{5.14b}$$

Again, coefficients that will later prove to be identically zero have been omitted from the above expansion. The non-zero coefficients are

$$u_\alpha^{(11)} = -u_{3,\alpha}^{(00)} - \hat{b}_\alpha^\beta u_\beta^{(00)}, \quad p^{(12)} = \hat{b}^{\alpha\beta}\Omega_{\alpha\beta}^{(00)}, \tag{5.15a}$$

$$p^{(01)} = 4u_3^{(22)} = 2a^{\alpha\beta}\Omega_{\alpha\beta}^{(00)}, \tag{5.15b}$$

$$p^{(10)} = -2a^{\alpha\beta}\Delta_{\alpha\beta}^{(20)} + \tfrac{1}{4}\hat{T}^2(2\hat{H}a^{\alpha\beta} + \hat{b}^{\alpha\beta})\Omega_{\alpha\beta}^{(00)}. \tag{5.15c}$$

By substituting (5.15) into (5.14) and using (5.12), we obtain

$$N^{\alpha\beta} = 4\mu T\mathscr{A}^{\alpha\beta\lambda\rho}\Delta_{\lambda\rho} + \mu T^3\mathscr{C}^{\alpha\beta\lambda\rho}\Omega_{\lambda\rho}, \tag{5.16a}$$

$$M^{\alpha\beta} = -\tfrac{1}{3}\mu T^3\mathscr{A}^{\alpha\beta\lambda\rho}\Omega_{\lambda\rho} \tag{5.16b}$$

where

$$\mathscr{C}^{\alpha\beta\lambda\rho} = \tfrac{1}{12}[8H\mathscr{A}^{\alpha\beta\lambda\rho} - 2a^{\alpha\beta}(3Ha^{\lambda\rho} + 2b^{\lambda\rho}) - a^{\alpha\rho}b^{\beta\lambda} - a^{\beta\rho}b^{\alpha\lambda} - 2(a^{\alpha\lambda}b^{\beta\rho} + a^{\beta\lambda}b^{\alpha\rho}) - 5a^{\lambda\rho}b^{\alpha\beta}]. \tag{5.17}$$

5.3. *Higher-order expansions*

When the asymptotic expansions described above are continued to higher order, it becomes necessary to apply the boundary conditions. Additional inhomogeneous terms then appear in the expressions for $N^{\alpha\beta}$ and $M^{\alpha\beta}$. In the membrane limit, these terms are

$$N^{\alpha\beta} = (\ldots) + \tfrac{1}{2}T\{P_3^+ + P_3^- + \gamma[a^{\lambda\rho}T|_{\lambda\rho} + K^2T]\}a^{\alpha\beta}, \tag{5.18a}$$

$$M^{\alpha\beta} = (\ldots) - \frac{T^3}{24}[2\rho f_3 a^{\alpha\beta} + (2Ha^{\alpha\beta} - b^{\alpha\beta})(P_3^+ + P_3^-) - \mathscr{D}^{\alpha\beta\lambda\rho}(P_\lambda^+|_\rho + P_\lambda^-|_\rho)], \tag{5.18b}$$

where

$$\mathscr{D}^{\alpha\beta\lambda\rho} = a^{\alpha\lambda}a^{\beta\rho} + a^{\alpha\rho}a^{\beta\lambda} + a^{\alpha\beta}a^{\lambda\rho} \tag{5.19}$$

and $(\ldots)$ denotes the results of the one-term expansion obtained previously. The analogous results for the inextensional limit are

$$N^{\alpha\beta} = (\ldots) + \tfrac{1}{2}T(P_3^+ + P_3^-)a^{\alpha\beta}, \quad M^{\alpha\beta} = (\ldots) + \tfrac{1}{20}T^2(P_3^+ - P_3^- + 4\gamma H)a^{\alpha\beta}. \tag{5.20}$$

5.4. *Composite expansions*

Uniformly valid composite expressions for $N^{\alpha\beta}$ and $M^{\alpha\beta}$ can now be obtained simply by gathering together the distinct terms that appear in the expressions for the membrane and inextensional limits. The results are

$$N^{\alpha\beta} = 4\mu T\mathscr{A}^{\alpha\beta\lambda\rho}\Delta_{\lambda\rho} + \mu T^3\mathscr{C}^{\alpha\beta\lambda\rho}\Omega_{\lambda\rho} + \tfrac{1}{2}T(P_3^+ + P_3^-)a^{\alpha\beta} + \tfrac{1}{2}\gamma T[a^{\lambda\rho}T|_{\lambda\rho} + K^2T]a^{\alpha\beta}, \tag{5.21a}$$

$$M^{\alpha\beta} = -\tfrac{1}{3}\mu T^3(\mathscr{A}^{\alpha\beta\lambda\rho}\Omega_{\lambda\rho} + \mathscr{B}^{\alpha\beta\lambda\rho}\Delta_{\lambda\rho}) - \tfrac{1}{24}T^3[2\rho f_3 a^{\alpha\beta} + (2Ha^{\alpha\beta} - b^{\alpha\beta})(P_3^+ + P_3^-) - \mathscr{D}^{\alpha\beta\lambda\rho}(P_\lambda^+|_\rho + P_\lambda^-|_\rho)] + \tfrac{1}{20}T^2(P_3^+ - P_3^- + 4\gamma H)a^{\alpha\beta}. \tag{5.21b}$$

The inhomogeneous terms on the second and third lines of (5.21a) and (5.21b) are those that appear at second and third order in the asymptotic expansions, respectively.

The final set of thin-sheet equations is now obtained by substituting (5.21) and (3.17) into (3.14). This yields three coupled equations for the velocity components U_i at the sheet midsurface.

6. Accuracy

The best way to evaluate the accuracy of the thin-sheet equations is to compare their solutions with exact analytical solutions of the equations of three-dimensional viscous flow. However, because few such solutions are available, we may instead compare solutions of simplified forms of the three-dimensional and thin-sheet equations that are valid for the special case of a shallow sheet with locally constant curvature. This approach is valid as long as both sets of equations are simplified in the same way, and has the advantage that it can be used for shells with arbitrary curvature.

As an illustration, consider the problem of a normally loaded shallow sheet treated in § 4. The solutions of the three-dimensional equations are given by (4.1) and (4.2), but with all numerators and denominators in (4.2) expanded to higher order in ϵ. The analogous set of thin-sheet equations is obtained by writing (3.14) and (5.21) with respect to orthogonal lines-of-curvature coordinates, making the shallow-sheet approximation $a_{11} = a^{11} = a_{22} = a^{22} = 1$, and setting $\gamma = P_-^j = 0$ and $P_+^j = P\delta_3^j$. The resulting equations are then solved by assuming that the velocity components depend on x_1 and x_2 as in (4.1). For comparison, we shall also determine the error inherent in an alternative set of thin-sheet equations based on the simplifed constitutive relations

$$N^{\alpha\beta} = 4\mu T \mathscr{A}^{\alpha\beta\lambda\rho}\Delta_{\lambda\rho}, \quad M^{\alpha\beta} = -\tfrac{1}{3}\mu T^3 \mathscr{A}^{\alpha\beta\lambda\rho}\Omega_{\lambda\rho}, \tag{6.1}$$

which are identical (*modulo* a time derivative) to the incompresible limit (Poisson's ratio $= 1/2$) of Koiter's (1970) constitutive relations for elastic shells.

Define the relative error of a quantity X as

$$\delta(X) = \frac{X_{TS} - X_{3D}}{X_{3D}}, \tag{6.2}$$

where X_{TS} and X_{3D} are the values of X predicted by the thin-sheet and the three-dimensional solutions, respectively. It suffices to calculate the errors $\delta(\Delta_\alpha^\alpha)$ and $\delta(\Omega_\alpha^\alpha)$ of the dilatation rate Δ_α^α and the total rate of change of curvature Ω_α^α. These errors are functions of four independent variables, which may be chosen as $\mathscr{K}$, $\mathscr{I}$, $\mathscr{G}/\mathscr{K}^2 \equiv r$, and ϵ. For simplicity, consider only the cases $r = 1/2$ (sphere) and $r = 0$ (cylinder); the errors for $r = -1/2$ (catenoid) are nearly identical to those for the sphere.

Let δ_R and δ_K denote the relative errors predicted using the full constitutive equations (5.21) and the 'Koiter' constitutive relations (6.1), respectively. For a spherical ($r = 1/2$) sheet, the errors depend only on $\mathscr{I} \equiv \mathscr{K}/\sqrt{2}$ and ϵ, and are, to order of magnitude,

$$\delta_R(\Delta_\alpha^\alpha) \sim \epsilon^2, \quad \delta_R(\Omega_\alpha^\alpha) \sim \frac{\epsilon^2[\mathscr{I}^4, \epsilon^2]}{[\mathscr{I}^2, \epsilon^2]}, \tag{6.3a}$$

$$\delta_K(\Delta_\alpha^\alpha) \sim \frac{\epsilon[\mathscr{I}^4, \epsilon^4]}{[\mathscr{I}^3, \epsilon^2\mathscr{I}, \epsilon^5]}, \quad \delta_K(\Omega_\alpha^\alpha) \sim \frac{\epsilon[\mathscr{I}^3, \epsilon^3]}{[\mathscr{I}^2, \epsilon^2]}, \tag{6.3b}$$

where [ ] denotes the maximum of the enclosed quantities. The vertical axis of figure 3(a) shows the power of ϵ to which the errors (6.3) are proportional when $\mathscr{I}$ is

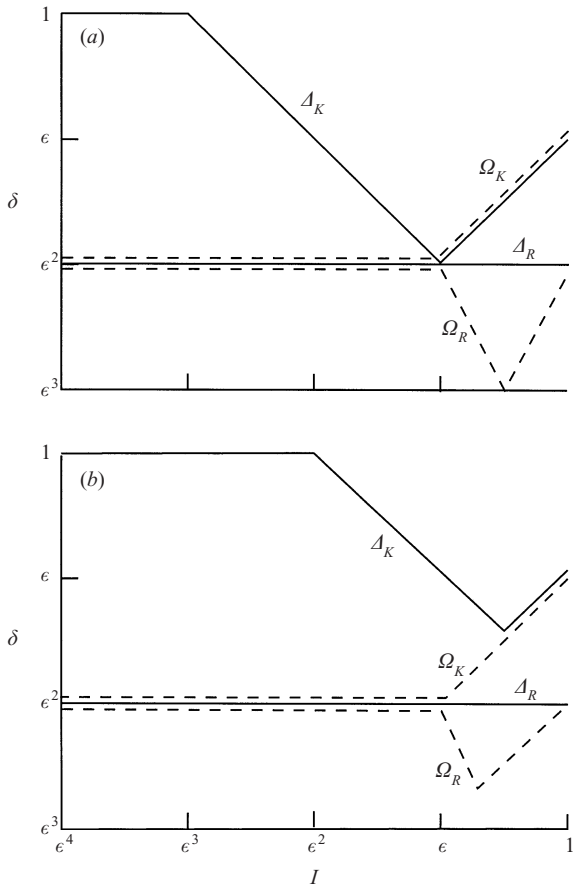

FIGURE 3. Orders of magnitude of the errors δ of the thin-sheet predictions of the stretching rate Δ_α^α and the bending rate Ω_α^α, relative to an analytical solution for a normally loaded shallow sheet. Verical axis shows the power of ϵ to which the error is proportional when $\mathscr{I}$ is proportional to the power of ϵ shown on the horizontal axis. Symbols Δ and Ω indicate the errors of Δ_α^α and Ω_α^α, respectively. Subscripts R and K denote the errors that result from using the full constitutive relations (5.21) and the 'uncoupled' constitutive relations (6.1), respectively. (*a*) Spherical sheet ($r = 1/2$); (*b*) cylindrical sheet ($r = 0$) with $\mathscr{K} = O(1)$.

proportional to the power of ϵ on the horizontal axis. Breaks in slope of the various lines occur where the dominant terms in the numerators and/or denominators of (6.3) change. The accuracy of the full thin-sheet equations is of order ϵ^2 or better in all cases. By contrast, the predictions of the simplified equations achieve this accuracy only for Ω_α^α when $\mathscr{I} \leqslant \epsilon$ and for Δ_α^α when $\mathscr{I} = \epsilon$.

The errors for a cylindrical sheet depend in general on both $\mathscr{I}$ and $\mathscr{K}$, which are independent quantities when $r \neq 1/2$. These errors are

$$\delta_R(\Delta_\alpha^\alpha) \sim \epsilon^2, \quad \delta_R(\Omega_\alpha^\alpha) \sim \frac{\epsilon^2[\mathscr{I}^3\mathscr{K}, \epsilon^2]}{[\mathscr{I}^2, \epsilon^2]}, \tag{6.4a}$$

$$\delta_K(\Delta_\alpha^\alpha) \sim \frac{\epsilon[\mathscr{I}^4, \epsilon\mathscr{I}^2\mathscr{K}, \epsilon^3\mathscr{K}, \epsilon^4]}{[\mathscr{I}^3, \epsilon^2\mathscr{I}, \epsilon^4\mathscr{K}, \epsilon^5],} \quad \delta_K(\Omega_\alpha^\alpha) \sim \frac{\epsilon[\mathscr{I}^3, \epsilon^3]}{[\mathscr{I}^2, \epsilon^2]}. \tag{6.4b}$$

The errors (6.4) are shown for $\mathscr{K} \sim 1$ in figure 3(*b*). Again, the errors δ_R of the full

thin-sheet equations are everywhere of order ϵ^2 or better, while those of the simplified theory achieve that accuracy only under restricted conditions.

In conclusion, recall that the shallow-sheet analytical solution from which the above error estimates were obtained is strictly speaking valid only when $\mathscr{K} \ll 1$. To test the range of validity of (6.3) and (6.4), I calculated the errors of the thin-sheet predictions of Δ_α^α and Ω_α^α relative to exact analytical solutions for harmonically loaded spherical and cylindrical sheets. The orders of magnitude of the resulting errors agree exactly with (6.3) and (6.4) for arbitrary $\mathscr{K}$, demonstrating that the shallow-sheet approximation yields correct error estimates even for sheets with $\mathscr{K} \sim 1$. Thus one may presume that the error estimates found in this section are generally valid, although a rigorous proof remains to be found.

7. Evolution of the sheet shape

Because the sheet is assumed to have no inertia, time plays no intrinsic role in its dynamics: the flow is determined entirely by the instantaneous geometry of the sheet and the distribution of loads acting on it. However, in most situations of interest both the geometry and the loading will themselves change with time. We therefore require additional kinematic equations that describe the evolution of the sheet shape and thickness.

Define the 'midsurface velocity' $\boldsymbol{V}$ as

$$\boldsymbol{V} \equiv V_\lambda \boldsymbol{a}^\lambda + V_3 \boldsymbol{a}^3 \equiv V^\lambda \boldsymbol{a}_\lambda + V^3 \boldsymbol{a}_3 = \frac{\partial \boldsymbol{r}_0}{\partial t}. \tag{7.1}$$

Because the midsurface is not a material surface, the midsurface velocity $\boldsymbol{V}$ is not exactly equal to the fluid velocity $\boldsymbol{U}$ evaluated at the midsurface. However, it is demonstrated in the Appendix that their difference vanishes in the thin-sheet limit $\epsilon \to 0$. This allows us to ignore the distinction between $\boldsymbol{U}$ and $\boldsymbol{V}$ in the derivation that follows, and to regard the midsurface as a material surface to within an error of order ϵ^2.

Consider first the rate of change of the metric tensor, namely

$$\frac{\partial a_{\alpha\beta}}{\partial t} \equiv \frac{\partial}{\partial t}(\boldsymbol{a}_\alpha \cdot \boldsymbol{a}_\beta). \tag{7.2}$$

Now

$$\frac{\partial \boldsymbol{a}_\alpha}{\partial t} = \frac{\partial}{\partial t}\boldsymbol{r}_{0,\alpha} = (V^\beta \boldsymbol{a}_\beta + V^3 \boldsymbol{a}_3)_{,\alpha}. \tag{7.3}$$

By expanding the derivatives, applying the Weingarten–Gauss relations

$$\boldsymbol{a}_{\beta,\alpha} = \Gamma^\lambda_{\beta\alpha} \boldsymbol{a}_\lambda + b_{\alpha\beta} \boldsymbol{a}_3, \quad \boldsymbol{a}_{3,\alpha} = -b^\beta_\alpha \boldsymbol{a}_\beta, \tag{7.4}$$

substituting the results into (7.2), and setting $\boldsymbol{V} = \boldsymbol{U}$, we obtain

$$\frac{\partial a_{\alpha\beta}}{\partial t} = 2\Delta_{\alpha\beta} \tag{7.5}$$

where $\Delta_{\alpha\beta}$ is defined by (5.1).

The rate of change of the curvature tensor is

$$\frac{\partial b_{\alpha\beta}}{\partial t} \equiv \frac{\partial}{\partial t}(\boldsymbol{a}_3 \cdot \boldsymbol{a}_{\alpha,\beta}). \tag{7.6}$$

Upon using (7.3), (7.4), and the relation

$$\frac{\partial \boldsymbol{a}_3}{\partial t} = -(V^\alpha b_{\alpha\beta} + V^3_{,\beta})\boldsymbol{a}^\beta \equiv \omega_\beta \boldsymbol{a}^\beta, \tag{7.7}$$

and setting $\boldsymbol{V} = \boldsymbol{U}$, (7.6) becomes

$$\frac{\partial b_{\alpha\beta}}{\partial t} = \Omega_{\alpha\beta} \tag{7.8}$$

where $\Omega_{\alpha\beta}$ is defined by (5.2).

The derivation of the evolution equation for the thickness T begins from the fact that the outer surfaces of the sheet are material surfaces. The convective derivative of a function $\Gamma = \Gamma(x_1, x_2, z, t)$ is (Fliert *et al.* 1995)

$$\frac{\mathrm{D}\Gamma}{\mathrm{D}t} = \frac{\partial \Gamma}{\partial t} + \left(\boldsymbol{u} - \boldsymbol{V} - z\frac{\partial \boldsymbol{a}_3}{\partial t}\right) \cdot \nabla \Gamma. \tag{7.9}$$

The quantity in parentheses in (7.9) is just the fluid velocity in a coordinate frame that translates with velocity $\boldsymbol{V}$ and rotates with angular velocity $\partial \boldsymbol{a}_3/\partial t$. The condition that particles on the surfaces $z = \pm T/2 \equiv \Gamma$ remain there is thus

$$u^\pm_3 - V_3 = \pm\frac{1}{2}\frac{\partial T}{\partial t} \pm \frac{1}{2h}(\mu^\rho_\rho \delta^\lambda_\alpha - \mu^\lambda_\alpha)\left(u^\alpha_\pm - V^\alpha \mp \frac{T}{2}\omega^\alpha\right) T_{,\lambda}, \tag{7.10}$$

where the definition (7.7) for ω_α and the relation $\nabla T = \boldsymbol{g}^\alpha T_{,\alpha}$ have been used.

By integrating the continuity equation (3.5) across the sheet we obtain

$$h^+u^+_3 - h^-u^-_3 = -I^\alpha|_\alpha + \tfrac{1}{2}(u^\alpha_+ + u^\alpha_-)T_{,\alpha} + (2H\delta^\lambda_\alpha - b^\lambda_\alpha)[J^\alpha|_\lambda - \tfrac{1}{4}T\,T_{,\lambda}(u^\alpha_+ - u^\alpha_-)], \tag{7.11}$$

where

$$I^\alpha = \int_{-T/2}^{T/2} u^\alpha \,\mathrm{d}z, \quad J^\alpha = \int_{-T/2}^{T/2} z u^\alpha \,\mathrm{d}z. \tag{7.12}$$

A second, independent expression for the quantity $h^+u^+_3 - h^-u^-_3$ can be formed by combining the two ($\pm$) parts of (7.10). Equating the two expressions and simplifying, we obtain

$$\left(1 + \frac{GT^2}{4}\right)\frac{\partial T}{\partial t} = 2HTV_3 + V^\alpha T_{,\alpha} - I^\alpha|_\alpha + (2Ha^{\alpha\lambda} - b^{\alpha\lambda})\left(J_\alpha|_\lambda - \frac{T^2}{4}T_{,\lambda}\omega_\alpha\right). \tag{7.13}$$

The evolution equation (7.13) is exact for a sheet of any thickness. However, it can be simplified considerably for a thin sheet by using the results of the shallow-sheet scaling analysis. First, this analysis shows that the term proportional to $T^2T_{,\lambda}$ in (7.13) is negligible relative to $V^\alpha T_{,\alpha}$ in both the membrane and inextensional limits. Second, by expanding u^α in powers of $\hat{z}$, we may write

$$I^\alpha \approx \int_{-T/2}^{T/2} (U^\alpha + u^\alpha_1\hat{z} + u^\alpha_2\hat{z}^2 + \ldots)\,\mathrm{d}z. \tag{7.14}$$

Only coefficients u^α_n with n even contribute to this integral. However, the scaling analysis shows that u^α_2, u^α_4, etc. are always smaller than U^α by a factor of at least ϵ^2, which implies $I^\alpha \sim TU^\alpha$. Using the definition (5.1) for $\Delta_{\alpha\beta}$ and noting that $GT^2 \ll 1$

for a thin sheet, we may write (7.13) as

$$\frac{\partial T}{\partial t} = -T\Delta^{\alpha}_{\alpha} + (2Ha^{\alpha\beta} - b^{\alpha\beta})J_{\alpha}|_{\beta}. \tag{7.15}$$

Turning now to the last term in the above equation, we find from the scaling analysis that it is negligible relative to $T\Delta^{\alpha}_{\alpha}$ in the membrane limit, but of the same order as $T\Delta^{\alpha}_{\alpha}$ in the inextensional limit. A simplified form of the term $J_{\alpha}|_{\beta}$ that is valid in the inextensional limit is obtained by noting that the dominant contribution to the integral J_{α} is made by the part of the lateral velocity that varies linearly across the sheet. The asymptotic expansion for an inextensional sheet shows that this part is $u_{\alpha} = z\omega_{\alpha}$, whence (7.15) becomes

$$\frac{\partial T}{\partial t} = -T\Delta^{\alpha}_{\alpha} + \tfrac{1}{12}(2Ha^{\alpha\beta} - b^{\alpha\beta})(T^3\omega_{\alpha})|_{\beta}. \tag{7.16}$$

The first term on the right-hand side of (7.16) represents the rate of thickening (thinning) associated with a net shortening (extension) of the sheet midsurface. The second term is non-zero only when there is a component of bending normal to a direction of non-zero principal curvature, and arises from the term proportional to z in the continuity equation (3.5).

8. Illustrative numerical solutions

We shall now study a number of simple model problems that illustrate the partitioning of thin-sheet deformation between stretching and bending modes. As for the shallow-sheet problem considered earlier, an appropriate measure of the intensities of stretching and bending is the rate of energy dissipation associated with each. The total (integrated across the sheet) dissipation rate $\Phi(x_1, x_2, t)$ per unit midsurface area can be determined in both the membrane and inextensional limits using the asymptotic expansions introduced above. The composite expression that is valid in both limits to within an error $\sim \epsilon^2$ is

$$\Phi = \tfrac{1}{2}\mu\mathscr{A}^{\alpha\beta\rho\lambda}(4T\Delta_{\alpha\beta}\Delta_{\rho\lambda} + \tfrac{1}{3}T^3\Omega_{\alpha\beta}\Omega_{\rho\lambda}) \equiv \Phi_s + \Phi_b. \tag{8.1}$$

The total dissipation rate is the sum of contributions due to bending (Φ_b) and stretching (Φ_s). The local dissipation number is thus

$$D(x_1, x_2, t) = \frac{\Phi_b}{\Phi_b + \Phi_s}. \tag{8.2}$$

8.1. *Deformation of viscous domes*

Axisymmetric viscous sheets appear in a variety of natural and artificial settings; perhaps the most common example is an air bubble at the surface of a viscous liquid such as molten glass or lava. In this subsection, the thin-sheet equations derived above will be used to study several idealized model problems for the axisymmetric deformation of a viscous dome under its own weight. The focus will be on the evolving partitioning of the deformation between stretching and bending modes, particularly in the form of buckling instabilities.

In solving such problems numerically, it is convenient to take the coordinate $x_1 \equiv s$ as the arclength along a meridian in the current configuration of the sheet. Axisymmetry implies that the flow does not vary in the x_2-direction. Let $(\xi(s,t), \zeta(s,t))$ be the (radial and axial) cylindrical coordinates of a point on the sheet. Then the

covariant components of the local metric and curvature tensors are (Niordson 1985, chap. 10)

$$a_{\alpha\beta} = \begin{pmatrix} 1 & 0 \\ 0 & \xi^2 \end{pmatrix}, \qquad b_{\alpha\beta} = \begin{pmatrix} \zeta''/\xi' & 0 \\ 0 & \xi\zeta' \end{pmatrix}, \tag{8.3}$$

where primes denote partial differentiation with respect to s. Let deformation of the sheet be driven by body forces whose components (per unit midsurface area) in the z- and s-directions are respectively $-\rho \boldsymbol{g} T(\cos\theta, \sin\theta)$, where $\boldsymbol{g}$ (reverting to standard notation) is the gravitational acceleration and θ is the sheet inclination from the horizontal. The outer surfaces of the sheet are assumed to be stress-free, and surface tension is neglected. Three different sets of end conditions will be considered, corresponding to a pole, a clamped end, and an end that slides without friction on a horizontal support:

$$U = W' = q^1 = 0 \quad \text{(pole)}, \tag{8.4a}$$

$$U = W = W' = 0 \quad \text{(clamped)}, \tag{8.4b}$$

$$U \sin\theta + W \cos\theta = q^1 = m^{11} = 0 \quad \text{(sliding)}. \tag{8.4c}$$

Solution of the numerical problem requires iteration between a two-point boundary value problem (determining the quasi-static response of the sheet to a specified distribution of loads) and an initial-value problem (advancing the sheet geometry forward in time). The most convenient forms of the quasi-static governing equations are the global force and torque balance equations (3.6) and (3.10) together with the definitions (3.13) and the constitutive relations (5.21), with $P^j_{\pm} = \gamma = 0$. These were rewritten as a system of six coupled first-order ordinary differential equations for the variables $U(s)$, $W(s)$, $\omega_1(s)$ (see (7.7)), $q^1(s)$, $n^{11}(s)$, and $m^{11}(s)$, and solved using the relaxation algorithm of Press *et al.* (1996). The sheet shape and thickness were advanced in time using a second-order Runge–Kutta algorithm. The accuracy of the relaxation algorithm was tested against analytical solutions for the deformation of a spherical sheet driven by a surface normal load having the form of an axisymmetric (order $m = 0$) spherical harmonic Y_l^0 of variable degree l. The accuracy of the time-stepping algorithm was checked by monitoring conservation of mass and by comparing two independent calculations of the sheet's total length.

Consider first the deformation of a sheet initially in the form of a hemispherical dome with radius L and normalized thickness $\epsilon = T_0/L = 0.01$, whose equatorial edge slides freely on a table. This is the viscous analogue of a classic problem in the theory of elastic shells (Landau & Lifshitz 1986, p. 57, Problem 2). The evolution of the sheet shape and dissipation number D are shown in figure 4, where time is normalized by the scale $\tau = \mu/L\rho g$. Because no shear stress or bending moment ($q^1 = m^{11} = 0$) is exerted on the sheet's equatorial edge, the initial ($t = 0$) flow approximates a pure membrane state ($D \approx 0$) that agrees closely (*modulo* a time derivative) with the analytical solution of Landau & Lifshitz (1986). Nevertheless, the latter is not an exact solution of the full thin-sheet equations, which contain bending terms that are neglected in the membrane equations of Landau & Lifshitz (1986). The sheet's initial near-membrane state is inherently unstable, and soon develops a large-amplitude fold or 'buckle' (figure 4*a*, $t/\tau = 0.3$). A similar instability occurs in a two-dimensional sheet whose ends are brought together at a constant velocity (Buckmaster *et al.* 1975). The complex structure of the flow within the sheet is revealed by the dissipation number D (figure 4*b*). At $t/\tau = 0.2$, an incipient bending instability with a well-defined characteristic wavelength is indicated by the values $D > 0$ in

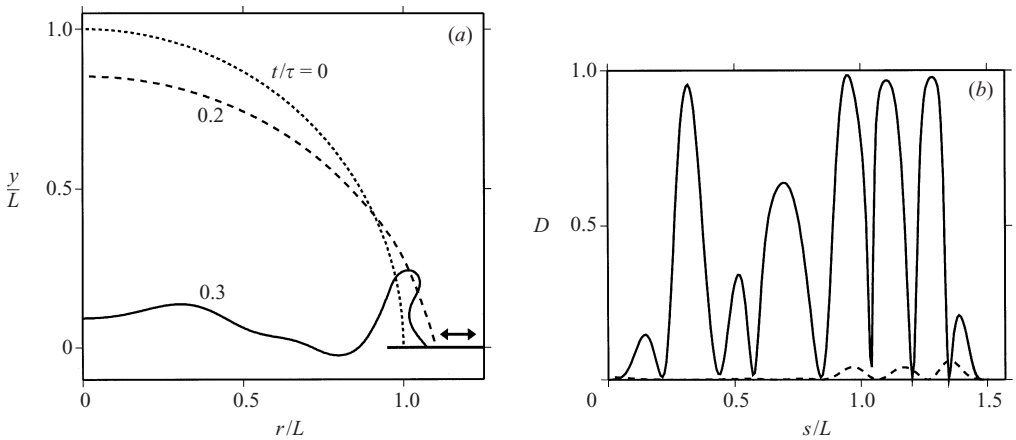

FIGURE 4. (*a*) Gravity-driven deformation of an initially hemispherical dome with radius L, normalized thickness $\epsilon \equiv T_0/L = 0.01$, and a freely sliding equatorial edge. Lines show the dome midsurface, and the time scale is $\tau = \mu/L\rho g$. (*b*) Dissipation number defined by (8.2), as a function of arclength s measured from the top of the dome along a meridian. Different line types are for the same times as in (*a*).

the sheet's lower half, while the rest of the sheet remains in a membrane state. By $t/\tau = 0.3$, however, the flow comprises regions of nearly pure stretching ($D \approx 0$) and nearly pure bending ($D \approx 1$) that alternate along the whole length of the sheet.

The influence of a different boundary condition is seen in figure 5, which shows the deformation of a dome with a clamped equatorial edge. The initial ($t = 0$) state of the sheet is nearly a pure membrane state everywhere except in a bending boundary layer at the clamped edge. Its width δ can be found from a simple scaling analysis. At the edge of the bending layer, the moment equation (3.14*b*) requires $M^{11}|_{11} \sim b_{11}N^{11}$. Because the boundary layer length scale is δ,

$$M^{11}|_{11} \sim \mu T^3 \partial_s^4 W \sim \frac{\mu T^3 W}{\delta^4}. \tag{8.5}$$

The length scale in the membrane region outside the boundary layer is L, whence

$$b_{11}N^{11} \sim L^{-1}(\mu T \Delta_{11}) \sim \frac{\mu T W}{L^2}. \tag{8.6}$$

Equating (8.5) and (8.6) yields $\delta \sim \epsilon^{1/2}L$. The same scaling is exhibited by bending boundary layers in elastic shells (Landau & Lifshitz 1986). As time progresses, a buckling instability develops near the clamped edge, and the effects of bending propagate progressively into the dome. The whole evolution occurs more rapidly than for a sliding dome (figure 4) because bending is important from the first instant.

Figure 6 shows what happens when the sliding dome of figure 4 is turned upside down to form a pendant hollow drop. The initial flow in the drop is identical (to within a minus sign) to that in the dome. The subsequent evolution, however, is entirely different, because the total strain rate Δ_α^α is now extensional everywhere. Bending instabilities are therefore suppressed, and the drop remains in a membrane state ($D \approx 0$) as it deforms under its own weight. The upper end of the drop thins most rapidly, and eventually pinches off.

The flows examined above were for simplicity assumed to be strictly axisymmetric. However, laboratory experiments on the related problem of a bursting viscous bubble

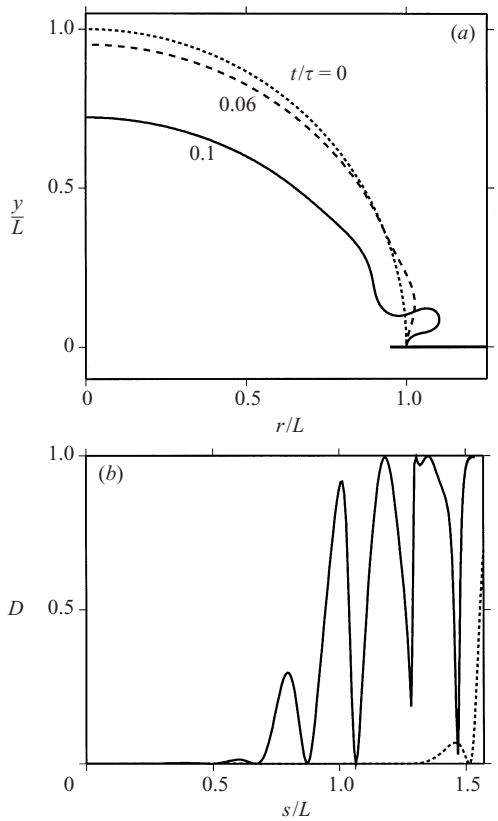

FIGURE 5. Same as in figure 4, but for a clamped equatorial edge.

show that the initial axisymmetric membrane (film-draining) state is unstable to a non-axisymmetric bending mode having the form of meridional ripples (Debrégeas, de Gennes & Brochard-Wyart 1998; Silveira, Chaïeb & Mahadevan 2000). The thin-sheet equations derived here could be used to model such non-axisymmetric flows, but that is beyond the scope of the present study.

8.2. *Buckling of viscous jets*

The folding or 'buckling' of a jet of viscous fluid falling upon a rigid surface is one of the most easily observed of all fluid mechanical instabilities. The best time to look is in the morning, when buckling can be seen in a stream of honey falling on toast or of shower gel falling on a washcloth. An understanding of viscous buckling is important in the food processing industry, where buckling of fluid jets during container filling causes unwanted entrainment of air into the product (Tome & McKee 1999). On a much larger scale, viscous buckling may occur when subducted oceanic lithosphere encounters a jump in viscosity and/or density at the boundary between the Earth's upper and lower mantles at 660 km depth (Griffiths & Turner 1988).

The classic early discussion of fluid buckling was that of Taylor (1969), who proposed that this instability, like its elastic analogue, requires a longitudinal compressive stress in the jet. Extensive experiments on buckling of both planar and axisymmetric jets were performed by Cruickshank & Munson (1981). They found that the critical height for the onset of instability is determined primarily by surface tension,

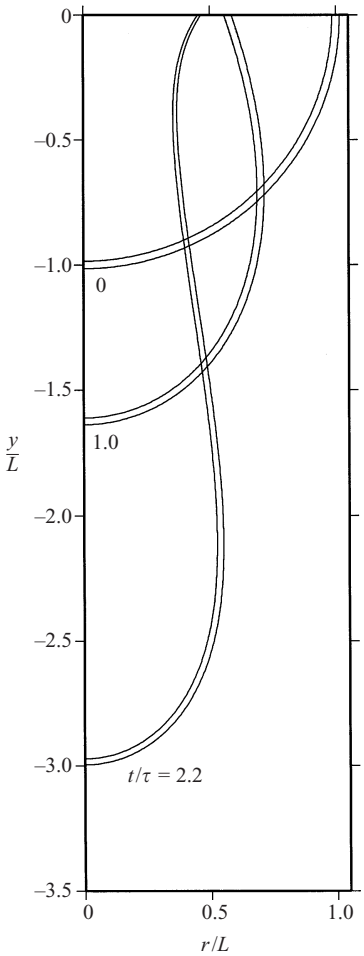

FIGURE 6. Same as figure 4(*a*), but with the dome inverted to form a pendant drop. The outer surfaces $z = \pm T/2$ of the sheet are shown at each time.

whereas the buckling frequency is influenced also by viscous, gravity and inertia effects. Further laboratory experiments were performed by Griffiths & Turner (1988), who studied the buckling of planar and axisymmetric jets incident on density and viscosity interfaces. The first theoretical studies of the phenomenon were limited to linear stability analysis of the onset of buckling. Cruickshank (1988) used a thin-layer theory to predict the critical height and frequency at onset, finding good agreement with experimental observations when empirical correction factors for geometrical and surface tension effects were included. Tchavdarov, Yarin & Radev (1993) proposed a more detailed theory for axisymmetric jets that included gravity and surface tension effects, and Yarin & Tchavdarov (1996) developed a similar theory for planar jets. More recent studies have focused primarily on the finite-amplitude behaviour of the instability. Tome & McKee (1999) used a marker-and-cell method to simulate the instability numerically without using thin-layer assumptions. Mahadevan, Ryu & Samuel (1998, 2000) proposed a scaling law for the coiling frequency of axisymmetric jets that agreed well with experimental measurements. Skorobogatiy & Mahadevan (2000) solved numerically a set of equations for the bending of an inextensible fluid

thread whose motion is confined to a plane, and proposed scaling laws for the folding length and frequency.

The thin-sheet equations derived here are a practical tool for modelling the buckling of planar jets that deform by both stretching and bending. As an example, consider the classic configuration of a jet issuing at speed U from a slot of width T_0 and falling towards a rigid plate at a distance L below the slot. Non-dimensionalization of the thin-sheet equations using the length scale L, velocity scale U, and time scale L/U shows that the problem involves the three dimensionless groups:

$$\epsilon = \frac{T_0}{L}, \quad B = \frac{\rho g L^2}{\mu U}, \quad S = \frac{\gamma}{\mu U}. \tag{8.7}$$

The groups B (buoyancy number) and S (inverse capillary number) are the characteristic ratios of the buoyancy and surface tension forces, respectively, to the viscous forces.

The numerical solution of this problem was obtained by the methods used in the previous subsection, using an arclength coordinate $x_1 \equiv s$ and metric and curvature tensors

$$a_{\alpha\beta} = \begin{pmatrix} 1 & 0 \\ 0 & 1 \end{pmatrix}, \quad b_{\alpha\beta} = \begin{pmatrix} \theta' & 0 \\ 0 & 0 \end{pmatrix}. \tag{8.8}$$

Terms involving surface tension were retained in (3.17) and (5.21). Finally, an idealized form of the boundary condition at the jet's leading edge was used, wherein the portion of the jet downstream of its contact with the plate is instantaneously removed each time a new contact is formed. Such a condition is appropriate because the portion of the jet downstream of a no-slip contact is irrelevant to the dynamics of the portion upstream. A similar boundary condition was used by Skorobogatiy & Mahadevan (2000).

Figure 7 shows the evolution of the buckling instability for $\epsilon = 0.1$, $B = 50$, and $S = 0$. The colours in each panel specify which of three distinct deformation states is dominant at each point in the sheet: membrane-dominated ($D \leqslant 1/2$) with axial extension (grey) or compression (white), and bending-dominated ($D > 1/2$; black). The number in the upper left corner of each panel is the dimensionless time $t' = tU/L$. The extruded jet initially deforms entirely by stretching, with $D = 0$ ($t' = 0.40$). When the jet reaches the plate, the boundary condition at its tip suddenly changes from free to clamped. The lower part of the jet is then in compression, while the upper part remains in extension ($t' = 0.48$). The compressional portion of the jet is unstable to small perturbations, which develop into a buckle comprising alternating intervals of membrane- and bending-dominated deformation ($t' = 0.53$). With increasing time, the jet develops a bipartite structure comprising a long and nearly vertical extensional 'tail' above a highly deformed bending-dominated region near the plate ($t' \geqslant 0.59$). The bending in the latter region generates a periodically alternating series of folds ($t' = 0.70$, 0.77). Figure 8 shows the horizontal position of the sheet midsurface at $y/L = -0.85$ as a function of time. After the decay of the initial transient, the jet settles down to a steady oscillatory state.

The numerically predicted buckling frequencies can be compared directly with the experimental observations of Cruickshank (1980), who measured the dimensionless frequency $2\pi f(T_0/g)^{1/2}$ as a function of ϵ^{-1} for fixed values of the parameters

$$F = \frac{\mu U}{\rho g T_0^2} \equiv \frac{1}{\epsilon^2 B}, \quad S' = \frac{\gamma}{\rho g T_0^2} \equiv FS. \tag{8.9}$$

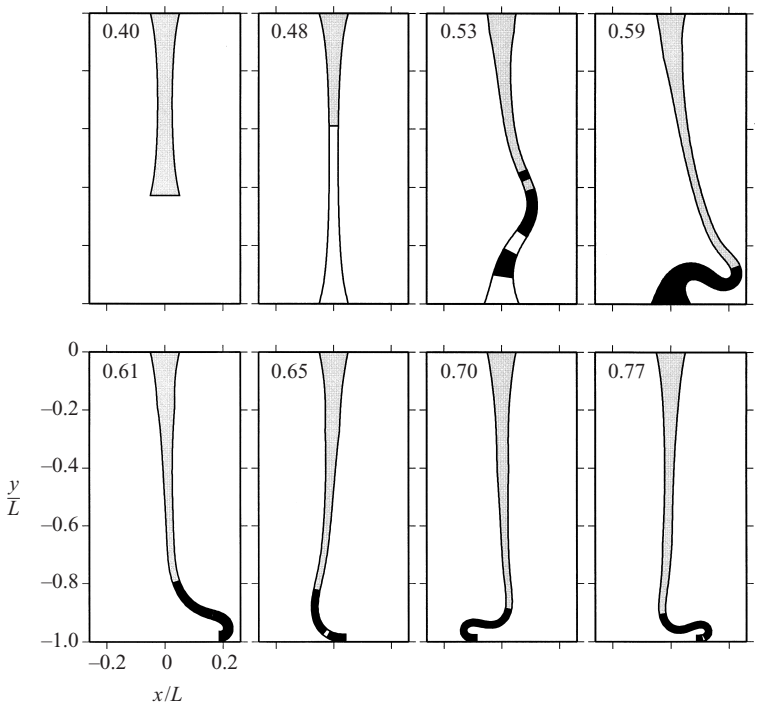

FIGURE 7. Buckling of a two-dimensional viscous jet with viscosity μ and density ρ, extruded downward with velocity U from a slot of width T_0 at $y = 0$ towards a rigid plate at $y = -L$. Case shown is for $L/T_0 \equiv \epsilon^{-1} = 10$ and $B = \rho g L^2/\mu U = 50$. Numbers at upper left of each panel are values of dimensionless time tL/U. Colours denote the type of deformation that accounts for $> 50\%$ of the local energy dissipation rate: extension (grey), compression (white), and bending (black).

Figure 9 shows the experimental data (a) and numerical predictions (b) for $S' = 0.59$ and $F = 41$ (open symbols) and $F = 144$ (solid symbols). Reliable numerical solutions could not be obtained for $\epsilon^{-1} > 35$ (with $F = 41$) or $\epsilon^{-1} > 50$ ($F = 144$.) The qualitative structure of the experimental and numerical curves is quite similar: in all cases, the frequency first decreases and then increases as ϵ^{-1} increases. However, the magnitudes of the numerical and experimental frequencies differ in some cases by a factor of up to about 2, probably due to the large departures from two-dimensionality in the laboratory experiments (see the Discussion below).

9. Discussion

The goal of this work has been to derive a theory that can predict the response of a thin viscous sheet of arbitrary shape and thickness to an arbitrary distribution of applied loads. The result can be regarded as a 'viscous shell theory', analogous to the better-known theory of elastic shells. But there are also several new results that are not to my knowledge to be found in the literature on elastic shells.

The first is an analytical solution for a shallow doubly curved sheet loaded by an harmonically varying normal stress, which provides a quantitative and easily comprehensible representation of how viscous sheets of arbitrary curvature respond to an applied load by a combination of stretching and bending. The shallow-sheet equations used here are of course not exact. Nevertheless, comparison of their solutions

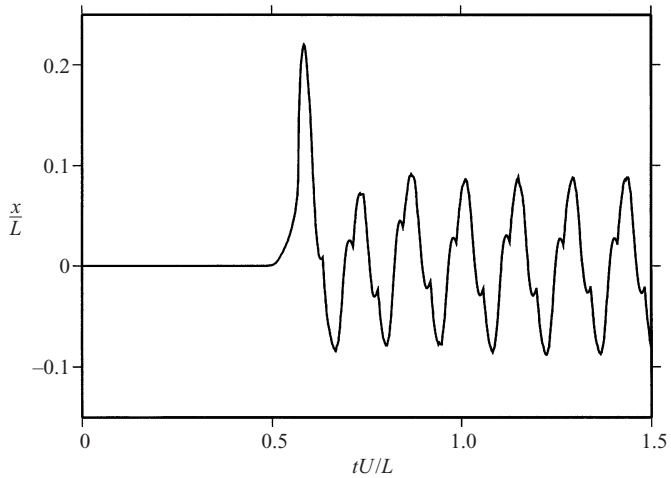

FIGURE 8. Horizontal position at $y/L = -0.85$ of the midsurface of the jet shown in figure 7, as a function of time.

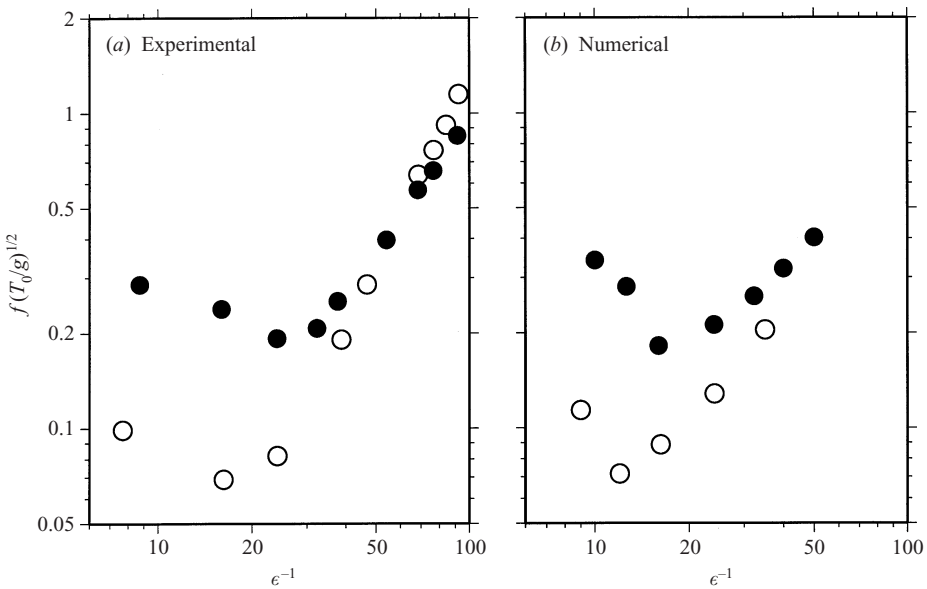

FIGURE 9. Comparison of experimentally observed buckling frequencies of planar jets (*a*; Cruickshank 1980, figure 24m) with numerical predictions using the thin-sheet model (*b*), for $S' = 0.59$ and $F = 41$ (open symbols) or $F = 144$ (solid symbols). F and S' are defined by (8.9).

with exact solutions of the three-dimensional Stokes equations shows that these differ only by numerical factors that do not affect the fundamental scalings involved. The shallow-sheet solution presented here is perhaps a useful alternative to the rather qualitative general discussions of response to loading that are typically found in books on elastic shell theory.

A second new result is the explicit expressions (5.10*b*) and (5.17) for the rheological tensors $\mathscr{B}^{\alpha\beta\rho\lambda}$ and $\mathscr{C}^{\alpha\beta\rho\lambda}$ that describe the coupling between bending and stretching of the sheet. Such terms are generally neglected in elastic shell theory, where 'uncoupled' constitutive relations such as (6.1) are typically used. Explicit expressions for the

coupling terms are satisfying from an asymptotic point of view, and their inclusion improves the accuracy of the thin-sheet equations (see below).

A third new result is the kinematic equation (7.16) for the sheet's rate of thickening. In elastic shell theory, changes in thickness are of little interest and generally ignored. They are however of great importance for viscous sheets that experience large deformations. Because (7.16) was derived with the aid of the shallow-sheet scaling analysis, it is asymptotically correct in both the membrane and inextensional limits.

The viscous membrane theory derived by Howell (1999) is a limiting case of the theory presented here, for a 'momentless' sheet in which shear stresses and bending moments are negligible. Howell (1999) considered deformation driven by buoyancy, surface tension, and an applied pressure difference ΔP. The force balance equations for this problem are obtained from (3.6) by setting $q^\alpha = P_+^j = 0$, $P_-^j = \Delta P \delta_3^j$ and using the constitutive relation (5.21a) for $N^{\alpha\beta} \approx n^{\alpha\beta}$. Retaining only leading-order terms, one finds

$$n_H^{\alpha\beta}|_\alpha + \tfrac{1}{2}\gamma T a^{\alpha\beta}(a^{\lambda\rho}T|_{\lambda\rho} + K^2 T)|_\alpha + \rho T f^\beta = 0, \tag{9.1a}$$

$$b_{\alpha\beta} n_H^{\alpha\beta} + \Delta P + 4\gamma H + \rho T f^3 = 0. \tag{9.1b}$$

where $n_H^{\alpha\beta} = 4\mu T \mathscr{A}^{\alpha\beta\lambda\rho} \Delta_{\lambda\rho}$ is the constitutive relation used by Howell (1999). Apart from differences in notation and non-dimensionalization, (9.1a) and (9.1b) are respectively identical to equations (A5) and (A6) of Howell (1999).

The theory derived here also has some relation to the theory of Newtonian surface or interfacial flow (Scriven 1960; Aris 1962; Edwards, Brenner & Wasan 1991). The latter theory considers an interface characterized by a linear relation between stress and strain, with two intrinsic viscosities that measure the resistance of the interface to dilatation and shear. However, because the interface is supposed to have vanishing thickness, the components of interfacial velocity are not functions of a normal coordinate. Newtonian interfaces are therefore essentially membranes with zero bending resistance, unlike the sheets of finite thickness considered here. A further difference is that the two viscosities of interface theory are independent interfacial parameters, not necessarily related to the viscosity of a bulk fluid phase.

As with any asymptotic theory, it is important to evaluate the errors involved relative to the exact governing equations and their solutions. The results of such an evaluation were presented in figure 3, which shows that the errors of the solutions of the thin-sheet equations derived here are uniformly of order ϵ^2 or better. By contrast, thin-sheet equations that use the uncoupled constitutive relations (6.1) achieve this accuracy only under restricted conditions, with errors reaching order unity in some cases. However, it is important to interpret this result fairly. When $\mathscr{I} \ll \epsilon$, most of the dissipation in the sheet is due to bending, so that errors in the stretching rate are of secondary importance. The converse is true for $\mathscr{I} \gg \epsilon$, when most of the dissipation is due to stretching. Accordingly, the most significant curves to compare in figure 3 are the dashed ones for $\mathscr{I} \ll \epsilon$ and the solid ones for $\mathscr{I} \gg \epsilon$. Evidently the equations based on the uncoupled constitutive relations do an excellent job in the inextensional limit $\mathscr{I} \ll \epsilon$. They do less well in the membrane limit $\mathscr{I} \gg \epsilon$, where their prediction of the stretching rate is significantly less accurate than that of the 'coupled' theory, although the error still vanishes in the limit $\epsilon \to 0$. The choice between the two theories will depend on whether one prefers accuracy (coupled constitutive relations) or simplicity (uncoupled).

The essence of the dynamics of thin viscous sheets is the complex partitioning of deformation between stretching (membrane) and bending (inextensional) modes.

Because the thin-sheet equations derived here include both effects, the partitioning of the deformation between them is automatically determined as part of any solution. It proves to be surprisingly complex and variable in space and time. Because the sheet inertia is negligible, the partitioning at a given instant depends only on three things: the sheet geometry, the distribution of loads acting on it, and the boundary conditions. Numerical solutions for gravitationally loaded spherical domes show that a crucial factor is whether a large-scale membrane state is compressional or extensional, as originally suggested by Taylor (1969). In the former case, the sheet is subject to buckling instabilities which develop on a time scale much shorter than that of the compression itself. The evolution is accelerated if the edge of the dome is clamped (figure 5), in which case a pure membrane state cannot exist and bending is (locally) important from the very beginning. The region influenced by bending is initially small, but quickly expands to fill the whole dome. In fact, this region has a complex structure comprising alternating intervals of nearly pure bending and nearly pure stretching. This structure is generally not evident from the shape of the dome midsurface alone, which is typically quite smooth on the scale of the bending/stretching 'waves' (figure 4). An entirely different behaviour obtains if the membrane state is extensional: buckling instabilities cannot develop and the membrane state persists (figure 6).

We have seen that the thin-sheet equations derived here can be used to model the well-known buckling instability of viscous jets incident on a rigid surface. While the numerically and experimentally determined buckling frequencies depend on ϵ^{-1} and the dimensionless extrusion rate F in very similar ways, their magnitudes can differ by up to a factor of 2 (figure 9). The most likely reason for this is the significant departures from two-dimensionality in the experiments of Cruickshank (1980), whose planar jets were extruded from slots of finite length d ($5T_0 \leqslant d \leqslant 15T_0$). Because of surface tension, the along-slot width of the jet decreases from d at the top to a much smaller value at the bottom (e.g. $\sim 0.2d$ in figure 3 of Cruickshank & Munson 1981). Consequently the effective values of ϵ^{-1} and F at the bottom of the jet, where the buckling takes place, are not the same as the nominal values at the top. The experimental situation could be more accurately modelled using the full two-dimensional thin-sheet equations, but that is beyond the scope of this paper.

The natural next step is evidently to explore the behaviour of fully three-dimensional sheets subject to loads with low or no symmetry. The shape of the sheet midsurface will then be a function of two independent spatial coordinates x_1 and x_2 and of time. Solution of such problems will require more sophisticated numerical methods than those used here.

This research was supported by the Centre Nationale de la Recherche Scientifique (France). I thank V. Barcilon, C. Calladine, A. Davaille, P. Howell, E. Sanchez-Palencia, and J. Simmonds for helpful discussions. Careful reviews by P. Howell, H. Stone and an anonymous referee helped greatly to improve the manuscript. Mathematical manipulations were carried out using Mathematica (Wolfram 1996).

Appendix. Midsurface velocity

Because the sheet midsurface is not material, the fluid velocity $\boldsymbol{U} \equiv \boldsymbol{u}(z = 0)$ there is not identical to the kinematically defined midsurface velocity $\boldsymbol{V} \equiv \partial \boldsymbol{r}_0/\partial t$. However, the shallow-sheet analytical solution of § 4 shows that $\boldsymbol{U} - \boldsymbol{V} \to 0$ as $\epsilon \to 0$. Differentiate (2.14) with respect to t and apply the definitions (7.1) and $\partial \boldsymbol{r}_\pm/\partial t = \boldsymbol{u}_\pm$ (because $\boldsymbol{r} = \boldsymbol{r}_\pm$ are material surfaces). Upon resolving the resulting vector equation

into lateral and normal components, one obtains

$$V^\alpha = u^\alpha_\pm \mp \tfrac{1}{2} T a^{\alpha\beta}\omega_\beta, \tag{A 1a}$$

$$V^3 = u^3_\pm \mp \frac{1}{2}\frac{\partial T}{\partial t}. \tag{A 1b}$$

Now consider the case of a shallow sheet of constant thickness, for which $a_{11} = a_{22} = 1$, $b_{11} = k_1$, $b_{22} = k_2$, $a_{12} = a_{21} = b_{12} = b_{21} = 0$, and $T = T_0$. After using these relations to simplify (7.13), substitute the result into (A 1*b*), and replace $\boldsymbol{u}$ in (A 1) by its shallow-sheet expansion (4.1) and (4.2). The velocities $V^i \equiv V_i$ are then determined by solving (A 1), noting that $\partial T/\partial t$ itself depends on V_3. The results are

$$\delta U_1 \equiv \frac{U_1 - V_1}{U_1} = -\frac{3\{\epsilon^2\mathscr{I} - \epsilon^3[3 + 2(\mathscr{G} - \mathscr{H} - \mathscr{K}^2)]\}}{2\{12[3\mathscr{I} + 2(\mathscr{K}_1 - \mathscr{K}_2)] - \epsilon^3\}}, \tag{A 2a}$$

$$\delta U_3 \equiv \frac{U_3 - V_3}{U_3} = \frac{\epsilon^2[2 + \mathscr{I}(3\mathscr{I} - 4\mathscr{H} - 1) + 4\mathscr{H} - 4\mathscr{K}^2]}{16}. \tag{A 2b}$$

The expression for $(U_2 - V_2)/U_2$ is obtained from (A 2*a*) by exchanging the subscripts 1 and 2. Equation (A 2*b*) shows that $\delta U_3 \sim \epsilon^2$ under all conditions. Equation (A 2*a*) shows that $\delta U_1 \sim \epsilon^2$ except for nearly flat sheets ($\mathscr{K} \ll \epsilon$), for which δU_1 is larger (e.g. $\delta U_1 \sim 1$ for $\mathscr{K} \sim \epsilon^3$). However, such errors are not significant because the lateral velocities in a normally loaded flat sheet are asymptotically small relative to the normal velocity.

REFERENCES

Aris, R. 1962 *Vectors, Tensors, and the Basic Equations of Fluid Mechanics*. Dover.

Benvenuto, E. 1991 *An Introduction to the History of Structural Mechanics. Part II: Vaulted Structures and Elastic Systems*. Springer.

Buckmaster, J. D., Nachman, A. & Ting, L. 1975 The buckling and stretching of a viscida. *J. Fluid Mech.* **69**, 1–20.

Budiansky, B. & Sanders, J. L. 1967 On the 'best' first-order linear shell theory. *Prog. Appl. Mech.* (W. Prager Anniversary Volume), pp. 129–140. Macmillan.

Calladine, C. R. 1983 *Theory of Shell Structures*. Cambridge University Press.

Ciarlet, P. G. 1998 *Introduction to Linear Shell Theory*. Gauthier-Villars.

Cruickshank, J. O. 1980 Viscous fluid buckling: a theoretical and experimental analysis with extensions to general fluid stability. PhD dissertation, Iowa State University, Ames, Iowa.

Cruickshank, J. O. 1988 Low-Reynolds-number instabilities in stagnating jet flows. *J. Fluid Mech.* **193**, 111–127.

Cruickshank, J. O. & Munson, B. R. 1981 Viscous fluid buckling of plane and axisymmetric jets. *J. Fluid Mech.* **113**, 221–239.

Debrégeas, G., de Gennes, P.-G. & Brochard-Wyart, F. 1998 The life and death of 'bare' viscous bubbles. *Science* **279**, 1704–1707.

Edwards, D. A., Brenner, H. & Wasan, D. T. 1991 *Interfacial Transport and Rheology*. Butterworth-Heinemann.

van de Fliert, B. W., Howell, P. D. & Ockenden, J. R. 1995 Pressure-driven flow of a thin viscous sheet. *J. Fluid Mech.* **292**, 359–376.

Goldenveizer, A. L. 1961 *Theory of Elastic Thin Shells*. Pergamon.

Goldenveizer, A. L. 1963 Derivation of an approximate theory of shells by means of asymptotic integration of the equations of the theory of elasticity. *Prikl. Mat. Mech.* **27**, 593–608.

Green, A. E. & Zerna, W. 1992 *Theoretical Elasticity*. Dover (referred to herein as GZ).

Griffiths, R. W. & Turner, J. S. 1988 Folding of viscous plumes impinging on a density or viscosity interface. *Geophys. J.* **95**, 397–419.

van der Hilst, R., Widyantoro, S. & Engdahl, E. R. 1997 Evidence for deep mantle circulation from global tomography. *Nature* **386**, 578–584.

Howell, P. D. 1996 Models for thin viscous sheets. *Eur. J. Appl. Maths* **7**, 321–343.

Howell, P. D. 1999 The draining of a two-dimensional bubble. *J. Engng Maths* **35**, 251–272.

Koiter, W. T. 1970 On the foundations of the linear theory of thin elastic shells. *Proc. Kon. Nederl. Akad. Wetensch.* **B73**, 169–195.

Landau, L. D. & Lifshitz, E. M. 1986 *Theory of Elasticity*, 3rd Edn. Pergamon.

Libai, A. & Simmonds, J. G. 1998 *The Nonlinear Theory of Elastic Shells.* Cambridge University Press.

Mahadevan, L., Ryu, W. S. & Samuel, A. D. T. 1998 Fluid 'rope trick' investigated. *Nature* **392**, 140.

Mahadevan, L., Ryu, W. S. & Samuel, A. D. T. 2000 Correction: Fluid 'rope trick' investigated. *Nature* **403**, 502.

Niordson, F. I. 1985 *Shell Theory*. North-Holland.

Novozhilov, V. V. 1959 *The Theory of Thin Shells*. P. Noordhoff.

Pearson, J. R. A. 1985 *Mechanics of Polymer Processing*. Elsevier.

Pearson, J. R. A. & Petrie, C. J. S. 1970*a* The flow of a tubular film. Part 1. Formal mathematical representation. *J. Fluid Mech.* **40**, 1–19.

Pearson, J. R. A. & Petrie, C. J. S. 1970*b* The flow of a tubular film. Part 2. Interpretation of the model and discussion of solutions. *J. Fluid Mech.* **42**, 609–625.

Press, W. H., Teukolsky, S. A., Vetterling, W. T. & Flannery, B. P. 1996 *Numerical Recipes in Fortran 77: The Art of Scientific Computing*, 2nd Edn, Cambridge University Press.

Ribe, N. M. 2001 Bending and stretching of thin viscous sheets. *J. Fluid Mech.* **433**, 135–160.

Sanchez-Palencia, E. 1990 Passages à la limite de l'élasticité tri-dimensionnelle à la théorie asymptotique des coques minces. *C. R. Acad. Sci. Paris* I **309**, 909–916.

Scriven, L. E. 1960 Dynamics of a fluid interface. *Chem. Engng Sci.* **12**, 98–108.

da Silveira, R., Chaïeb, S. & Mahadevan, L. 2000 Rippling instability of a collapsing bubble. *Science* **287**, 1468–1471.

Skorobogatiy, M. & Mahadevan, L. 2000 Folding of viscous sheets and filaments. *Europhys. Lett.* **52**, 532–538.

Taylor, G. I. 1969 Instability of jets, threads, and sheets of viscous fluid. *Proc. 12th Intl Congr. Appl. Mech., Stanford, 1968*, pp. 382–388. Springer.

Tchavdarov, B., Yarin, A. L. & Radev, S. 1993 Buckling of thin liquid jets. *J. Fluid Mech.* **253**, 593–615.

Tome, M. F. & McKee, S. 1999 Numerical simulation of viscous flow: buckling of planar jets. *Intl J. Numer. Meth. Fluids* **29**, 705–718.

Wolfram, S. 1996 *The Mathematica Book*, 3rd Edn. Wolfram Media/Cambridge University Press.

Yarin, A. L. & Tchavdarov, B. M. 1996 Onset of folding in plane liquid films. *J. Fluid Mech.* **307**, 85–99.